ORIENTATION DEPENDENCE OF DIELECTRIC SUSCEPTIBILITIES AND SWITCHING CHARACTERISTICS IN EPITAXIAL FERROELECTRIC THIN FILMS

BY

RUIJUAN XU

THESIS

Submitted in fulfillment of the requirements
for the degree of Master of Science in Materials Science and Engineering
in the Graduate College of the
University of Illinois at Urbana-Champaign, 2014

Urbana, Illinois

Adviser:

Professor Lane W. Martin

ABSTRACT

When subjected to low electric field, domain walls play an important role in determining the response of ferroelectrics to applied stimuli. While contributions to ferroelectric properties from the intrinsic response of the polarization within a domain and so-called extrinsic contributions from the motion of domain walls have been studied, the non-motional or stationary contribution from the material within the finite width of the domain wall itself has been particularly difficult to understand. When subjected to high electric field, switchable polarization makes ferroelectrics a critical component in memories, actuators, and electro-optic devices and potential candidates for nanoelectronics. Although many studies of ferroelectric switching have been undertaken, much remains to be understood about switching in complex domain structures and in devices. In the present work, in order to investigate the low field dielectric response, using a combination of phenomenological models, thin-film growth, and multi-scale characterization we have probed model versions of (001)-, (101)-, and (111)-oriented epitaxial films. In particular, we observe that (111)-oriented films, in which the extrinsic contributions from the high density of 90° domain walls are frozen out, exhibit permittivity values approximately 3-times larger than that expected from the intrinsic response alone. This discrepancy can only be accounted for by considering a stationary contribution to the permittivity from the domain wall volume of the material that is 6-77.5-times larger than the bulk response and is consistent with recent predictions of the enhancement of susceptibilities within 90° domain walls. In order to investigate the high field switching characteristics, a combination of thin-film epitaxy, macro- and nanoscale property and switching characterization, and molecular dynamics simulations are used to elucidate the nature of switching in $PbZr_{0.2}Ti_{0.8}O_3$ thin films. Differences are demonstrated between (001)-/(101)- and (111)-oriented films, with the latter exhibiting complex, nanotwinned ferroelectric domain structures with high densities of 90° domain walls and considerably broadened switching characteristics. Molecular dynamics simulations predict both 180° (for (001)-/(101)-oriented films) and 90° multi-step switching (for (111)-oriented films) and these processes are subsequently observed in stroboscopic piezoresponse force microscopy. These results have

implications for our understanding of ferroelectric switching and offer opportunities to change domain reversal speed. Our work also offers new insights into the microscopic origin of dielectric enhancement and provides a pathway to engineer the dielectric response of these materials.

To my dearest grandparents

ACKNOWLEDGEMENTS

In the past three years in Urbana-Champaign, I experienced the most failures compared to any previous period of my life, from both the research and life. I am still the fortunate one because after going through so many tough processes I think I learned more than what the success can give. I am also fortunate because a lot of people have ever helped and supported me, without whom I could not complete these three years' study and work.

First, I would like to thank my advisor, Prof. Lane W. Martin, who gave me an opportunity working in the area of oxide materials. Without his guidance and support, I could not finish the work in this thesis and publish them in top journals. I am very grateful to him that he teaches me how to become a successful graduate student and a good scientist from any detailed aspect including research philosophy, work ethic, time management, and writing/presentation skills. His leadership, interpersonal skills, and successful lab management also provide a role model to every student in their professional career life.

Second, I am very grateful to my family who always support and understand me in those bad days of my life. I am so deeply guilty that in the past three years I only spent one month with them and forever missed the last chance to meet my dearest grandmother. Thank them again for their understanding and forgiveness. I am also so grateful to my Fiancé Yin, who always makes me feel happy and not lonely. Without his company, I could not bear all those unhappiness and loneliness in US.

Last but not least, I would like to thank all the labmates from Prof. Martin's lab for their useful discussions on my work and kind help on my experiment and theoretical calculations. In addition, sincere thanks also to my collaborators Shi Liu, Dr. Ilya Grinberg, and Prof. Andrew Rappe from University of Pennsylvania. The numerous discussions with them have helped me gain better understandings in physics of ferroelectrics.

TABLE OF CONTENTS

CHAPTER 1

INTRODUCTION

In this chapter, we provide a brief introduction to the physics of ferroelectricity including a review of the mechanism of ferroelectricity, ferroelectric domain structures, and ferroelectric susceptibilities. In addition, the chapter concludes with a summary of the organization of the rest of the thesis.

1.1 Introduction to Ferroelectrics

Ferroelectric materials are increasingly being considered as critical components in next generation logic devices [1], non-volatile memories [2,3], actuators and sensors [4], and electro-optic elements for waveguide devices [5]. Of the 32 crystal classes of materials, 11 possess centers of symmetry and hence no polar properties. Of the remaining 21, all but one when subjected to a stress exhibit electrical polarity and are hence called *piezoelectric*. Of the 20 piezoelectric crystal classes, 10 show a unique polar axis. These crystals are called *polar* because they possess a spontaneous polarization. One can, however, often detect the presence of a spontaneous polarization by studying the temperature dependent changes in polarization which results in the flow of charge to and from the surfaces. This is known as the *pyroelectric effect* and these 10 polar crystal classes are often referred to as the *pyroelectric classes*. Ferroelectric materials possess a spontaneous polarization which can be switched from one state to another under the application of the external electric field and they also undergo a phase transition from its high temperature parent paraelectric state to the low temperature ferroelectric state.

Any lattice of oppositely signed point charges is inherently unstable and relies on short-range interactions between adjacent electron clouds in the material to stabilize the structure. In ferroelectric materials these interactions result in the formation of a double-well potential that stabilizes a distorted structure over the symmetric structure. In the case of classic perovskite ferroelectrics like $PbTiO_3$ and $BaTiO_3$ the Ti 3*d* –O 2*p* orbital hybridization is essential for stabilizing the ferroelectric distortion. It has also been found that most perovskite ferroelectrics have B-site ions that are formally d^0 in nature and thus the lowest unoccupied energy levels are the *d* states and they tend to hybridized with the O 2*p* orbitals resulting in the double well potential. Additionally, another mechanism for ferroelectricity is the stereochemical activity of ns^2 lone pairs of electrons such as materials like $PbTiO_3$, where Pb and Ti states hybridize, leading to a large strain that stabilizes the tetragonal phase.

1.2 Ferroelectric Domain Structures

The formation of domain structures is a result of minimizing the elastic and electrostatic energy of a ferroelectric system. It is very important to study such domain formation in ferroelectrics since it has a profound influence on the susceptibilities and switching behavior of these materials. Here we focus on an important ferroelectric material, tetragonal $PbZr_{0.2}Ti_{0.8}O_3$ that has been studied extensively. In the family of $PbZr_{1-x}Ti_xO_3$ materials, $PbZr_{0.2}Ti_{0.8}O_3$ is a well-known tetragonal ferroelectric, which can exhibit only a few possible domain structures depending on the nature of epitaxial strain when grown epitaxially on a (001)-oriented substrate – monodomain films of *c*-domains, mixed in-plane and out-of-plane *c/a/c/a* domain structures, or all in-plane oriented $a_1/a_2/a_1/a_2$ domain structures. In addition to the strain tuning, varying the film thickness can also change the domain structure. For example, below the critical thickness of domain formation, $PbZr_{0.2}Ti_{0.8}O_3$ thin films with monodomain have been observed when grown on $SrTiO_3$ substrates; however, when the thickness is increased, polydomain structures have typically been observed. An alternative approach that has been considerably less studied is to manipulate the film orientation, in chapter 2, the effects of film orientation on domain structures of $PbZr_{0.2}Ti_{0.8}O_3$ thin films will be discussed in details.

1.3 Ferroelectric Susceptibilities

The search for ferroelectric materials with high electric field (dielectric), stress (piezoelectric), and thermal (pyroelectric) susceptibilities has garnered much attention in recent years as these materials serve as the foundation for modern memory [6], sensor and actuator [7, 8] , and thermal imaging and infrared detector systems [9, 10, 11]. To ultimately understand the nature of such responses, it is imperative to understand the various contributions to the susceptibility in these complex materials. Since ferroelectrics typically possess complex domain structures with homogeneously polarized domains separated by domain walls, the susceptibility consists of two major contributions. The first is the so-called intrinsic contribution arising from the change in the polarization to an applied stimulus within the bulk of the domains. The second is the so-called extrinsic contribution which refers to the contribution that arises due to the motion of domain walls under an applied stimulus [12, 13, 14, 15, 16, 17, 18, 19, 20]. Beyond

the motional extrinsic contribution from domain walls, various reports have highlighted the potential importance of what has been alternatively called a stationary or frozen contribution that arises from the response of the volume of the ferroelectric material within the finite width of the domain walls to an applied stimulus irrespective of any lateral displacements or deformations of the wall [21, 22, 23, 24].

As early as the 1970s, the importance of these various contributions to ferroelectric susceptibility was already under investigation. Early studies of dielectric permittivity in $BaTiO_3$ revealed what was suspected to be a large domain wall contribution to permittivity even at excitation fields where the lateral displacement of domain walls was unlikely [25]. Subsequent theoretical studies probed the possibility of the weak measurement fields inducing nuclei on the existing domain walls and thus promoting protuberance-type oscillation but revealed that these could only account for a small fraction of the observed permittivity change [26]. Soon after this it was conjectured that the material within the domain walls themselves could possess significantly enhanced dielectric permittivity [21, 27]. Such models suggested that 180° domain walls in $BaTiO_3$ could possess permittivity almost an order of magnitude larger than the bulk of the domains. More recently, advanced Ginzburg-Landau-Devonshire (GLD) models have probed the role of polarization gradients near 90° domain walls in $BaTiO_3$ to suggest that such domain walls could give rise to an enhancement of susceptibilities between 1.1 to 1000-times larger than the bulk [24]. Despite these predictions as to the potential importance of such stationary contributions, it has proven difficult to quantitatively measure and isolate the stationary contribution (possibly because of the small relative volume associated with domain walls in most samples). In turn, much work on polydomain ferroelectrics has neglected the stationary contribution and focused solely on enhancements that can be explained by motional extrinsic contributions. Regardless, it is clear that in order to fully understand the response of a ferroelectric to an applied stimulus, one must consider not only the response of the bulk material within the domains but also the response of the domain walls to the applied stimuli.

1.4 Organization of the Thesis

The remainder of the thesis consists of three chapters.

In chapter 2, we introduce the details of growth of epitaxial thin films on substrates with various orientations. Furthermore, we also provide details of crystal and domain structure characterization via x-ray diffraction and piezoresponse force microscopy, respectively.

In chapter 3, we use a combination of phenomenological models, thin-film growth, and multi-scale characterization to probe the dielectric properties of model versions of (001)-, (101)-, and (111)-oriented epitaxial PZT films. We first develop phenomenological GLD modeling to study the dielectric properties of (001)-, (101)-, and (111)-oriented epitaxial PZT films. Then we move on to the investigation of dielectric properties in the model versions of films via experiment. And we specifically discuss the mechanism of the enhancement of low field dielectric properties in (111)-oriented PZT thin films.

In chapter 4, we use a combination of thin-film epitaxy, macro- and nanoscale property and switching characterization, and molecular dynamics simulations are used to elucidate the nature of switching in $PbZr_{0.2}Ti_{0.8}O_3$ thin films. We first introduce the measurement of macro-scale high field switching properties of PZT thin films. Then we move on to the investigation of switching characteristics for each film orientation using molecular dynamics simulations. Furthermore we use Piezoresponse force microscopy to study the difference of local-scale switching characteristics of PZT thin films.

In chapter 5, we summarize the major findings of the current work and provide suggestions for future work to build on the findings presented here.

CHAPTER 2

GROWTH AND CHARACTERIZATION OF (001)-, (101)-, AND (111)-ORIENTED PZT THIN FILMS

In this chapter, we present the growth of (001)-, (101)-, and (111)-oriented PZT thin films via pulsed-laser deposition. We also discuss the detailed characterization of crystal and domain structures of these model versions of films using x-ray diffraction and piezoresponse force microscopy. We show that the domain structure can be dramatically manipulated by varying the film orientation and the domain wall density is significantly increased in (111)-oriented films.

2.1 Growth of Epitaxial PZT Thin Films

Recent advances in thin-film synthesis have enabled the manipulation of structure and properties of ferroelectric thin films [28,29]. For example, in the tetragonal ferroelectric $PbZr_{0.2}Ti_{0.8}O_3$ both the domain structure [30,31] and properties (*i.e.*, dielectric [32,19], piezoelectric [33], and pyroelectric [34,35]) can be dramatically tuned by varying epitaxial strain, film thickness, electrical boundary conditions, and other parameters. To date, the majority of work on such films has focused on (001)-oriented heterostructures, where the possible domain structures have been theoretically predicted [35,36] and observed [35,37]. How these domain structures evolve in other film orientations, however, has not been widely probed [38,39]. Studies of single-crystal ferroelectrics, however, where it is possible to apply the stimulus field along different crystallographic directions, have demonstrated that a poling field that is not purely along the bulk polarization direction produces increased domain wall density and enhanced dielectric [40] and piezoelectric [41] responses. Similar studies on thin-film samples have not been completed.

Here we grow 150 nm $PbZr_{0.2}Ti_{0.8}O_3$ / 10 nm $SrRuO_3$ or $La_{0.7}Sr_{0.3}MnO_3$ / $SrTiO_3$ (001), (110), and (111) heterostructures via pulsed-laser deposition. The growth of the $PbZr_{0.2}Ti_{0.8}O_3$ was carried out at an oxygen pressure of 200 mTorr at 635°C with a laser fluence of 0.9-1.0 J cm^{-2} and a laser repetition rate of 3 Hz. The growth of bottom electrodes $SrRuO_3$ and $La_{0.7}Sr_{0.3}MnO_3$ was accomplished at an oxygen pressure of 100 mTorr and 200 mTorr, respectively, at 645°C with a laser repetition rate of 12 Hz and 3 Hz, respectively. After the growth, the samples were cooled at 5°C min^{-1} in an oxygen pressure of 760 mTorr.

2.2 Structural Characterization of PZT Thin Films

We characterized the crystal structure of various film orientations via x-ray diffraction reciprocal space mapping studies. On-axis reciprocal space maps measured about the $SrTiO_3$ 002-, 110-, and 111-diffraction conditions are provided [Fig. 2.1]. In (001)-oriented films, a majority peak corresponding to the 002-diffraction condition and a minority peak corresponding to the 200-diffraction condition of the

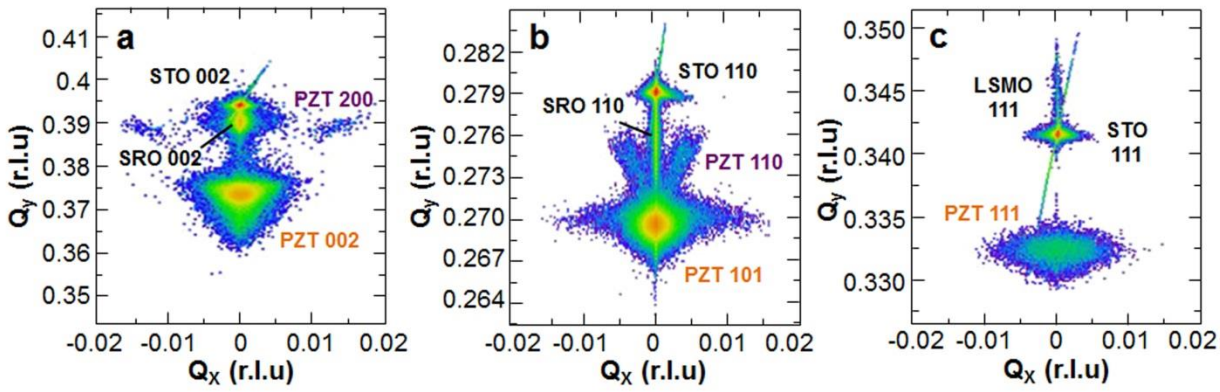

Figure 2.1: On-axis reciprocal space maps measured about the $SrTiO_3$ 002-, 110-, and 111-diffraction conditions for (a) (001)-oriented heterostructures with a majority peak corresponding to the 002-diffraction condition and a minority peak corresponding to the 200-diffraction condition of the $PbZr_{0.2}Ti_{0.8}O_3$ which represent *c* and *a* domains, respectively; (b) (101)-oriented heterostructures with diffraction peaks corresponding to the 101- and 110-diffraction conditions which represent the majority and minority domains of $PbZr_{0.2}Ti_{0.8}O_3$, respectively; (c) (111)-oriented heterostructures with only one broad diffraction peak which confirms the degeneracy of various polarization variants in this orientation that possess uniform out-of-plane lattice spacing.

$PbZr_{0.2}Ti_{0.8}O_3$ are observed and correspond to the presence of *c* and *a* domains, respectively [Fig. 2.1 a]. The (101)-oriented films also exhibit two diffraction peaks corresponding to the 101- and 110-diffraction conditions and to the majority and minority domains of $PbZr_{0.2}Ti_{0.8}O_3$ described above, respectively [Fig. 2.1 b]. In (111)-oriented films, however, there is only one broad diffraction peak [Fig. 2.1 c], which further confirms the degeneracy of various polarization variants in this orientation which possess uniform out-of-plane lattice spacing. These reciprocal space mapping studies also provide further evidence supporting the observed domain structures from the PFM analysis.

2.3 Ferroelectric Domain Structures of PZT Thin Films

The domain structure of the films was probed via piezoresponse force microscopy (PFM). In (001)-oriented $PbZr_{0.2}Ti_{0.8}O_3$ thin films, we observe *c/a/c/a* domain structures that are commonly seen in tetragonal ferroelectric thin-films and consist of majority out-of-plane polarized *c* and in-plane polarized *a* domains separated by 90° domain walls [Fig. 2.2 a] [42]. The density of 90° domain walls is known to increase with increasing tensile strain which corresponds to an enhancement of the motional extrinsic contribution to the low-field permittivity in (001)-oriented films [19,52,53]. Considerably less work in this vein, however, has been undertaken for (101)- and (111)-oriented films [43].

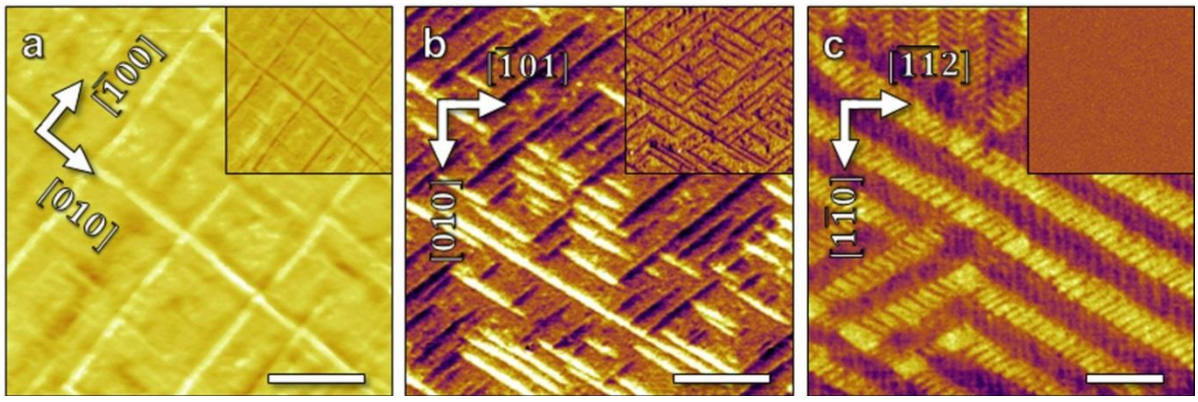

Figure 2.2: Piezoresponse force microscopy images showing lateral (mixed phase (θ) and amplitude (A), A·cosθ) and vertical (mixed phase (θ) and amplitude (A), A·cosθ, inset) contrast for equilibrium domain structures of (a) (001)-, (b) (101)-, and (c) (111)-oriented $PbZr_{0.2}Ti_{0.8}O_3$ thin films. Scale bar: 500 nm.

Thus, here we provide detailed studies of domain structures and permittivity in (101)- and (111)-oriented films. In the (101)-oriented films the PFM images reveal a mixed domain pattern where the majority of the sample is made up of domains with polarization along the [001] which is oriented at an angle of ~43.6° from the plane of the film, while the remaining structure consists of stripe-like domains possessing only in-plane polarization components pointing along the [010] or [$0\bar{1}0$] [Fig. 2.2 b]. In (111)-oriented films, however, a complex metastable domain structure was observed in the as-grown state and in order to probe the equilibrium domain structure the samples were poled with a series of +/- 6 V biases applied locally to a PFM tip to switch a 2.5 μm × 2.5 μm region (samples were switched between 2-6 times). Following such poling a complex, ordered nanotwinned domain pattern with a high density of uncharged 90° domain walls was observed [Fig. 2.2 c]. The observed domain structure is the result of the tiling of three types of domain bands, separated by 120° with average domain band widths of ~300 nm. Within each domain band, the domain structure consists of a mixture of all three degenerate polarization variants (pointing along the [$0\bar{1}0$], [$00\bar{1}$], and [$\bar{1}00$], which are oriented at an equal angle of ~33.9° from the plane of the film) distributed into two sub-bands, with each sub-band being made-up of only two of the polarization variants, consistent with prior predictions [44]. Regardless of the film orientation, the PFM studies indicate the presence of no 180° domain walls as a result of the preferential out-of-plane direction of the polarization which is induced by the asymmetric electrical boundary conditions (i.e., the

presence of a bottom electrode). Thus, in comparison to traditional bulk ceramic samples, these films provide a well-characterized, model system exhibiting controllable domain structures possessing only single type of domain walls (i.e., 90°).

The PFM analysis further allows for the direct quantification of the domain structures – in particular the determination of the domain wall density (λ, defined as the total length of domain walls in a given area) and the volume fraction of minority domains ($\phi_{\min}$, defined as the volume fraction of the domain type which possesses the smallest population among all polarization variants in the case of a poled film). In (001)- and (101)-oriented films, the minority domain represents the domain with the polarization pointing in the plane-of-the-film (along the [100], [010] and [010], [$0\bar{1}0$], respectively). Due to symmetry in (111)-oriented films, however, one can select any of the three polarization variants as the minority domain as they all form an equal angle with the normal direction of the substrate and occur in equal fractions. To briefly explain the analyzing process, image analysis of the PFM domain structure images allows for the selection and measurement of the perimeter and area of all domain types and hence direct measurement of λ and the area fraction of the domains. To estimate $\phi_{\min}$, we have assumed a uniform width of the domains throughout the thickness of the film [45-48]. It should be noted that this assumption matches the assumptions of the GLD models (or, in other words, matches the ideal domain structure that would be predicted from such models), but might slightly overestimate the volume density if the domains are more wedge-shaped [49]. Regardless, this potential slight discrepancy has little to no impact on the overall conclusion of the data below. The values of λ and $\phi_{\min}$ are provided [Table 1]. From this analysis, it is clear that the (111)-oriented films possess domain wall densities that are at least 3-5.5-times the values for (001)- and (101)-oriented films and that the experimentally observed $\phi_{\min}$value is consistent with the degeneracy of the three polarization variants in (111)-oriented films calculated from the GLD models.

TABLE 2.1: Domain structure analysis of $PbZr_{0.2}Ti_{0.8}O_3$ films: Line density of 90° domain walls (λ) and volume fraction of minority domains (ϕ_{min}) measured for (001)-, (101)-, and (111)-oriented fils.

Orientation	λ (μm^{-1})	ϕ_{min} (%)
(001)	8.91	15.3
(101)	16.3	19.9
(111)	48.9	33.3

This work reveals that in addition to the use of epitaxial strain [50], film thickness [42], and film composition [51] to manipulate domain structures in ferroelectrics, film orientation is another effective route by which to control the domain structure and domain wall density. In fact, (111)-oriented films enable the study of domain structures and densities not possible in other orientations at these film thicknesses. This enhanced density of domain walls will boost the contribution of such features to the overall response to applied stimuli. Furthermore, due to the degeneracy of the different domain variants the extrinsic contribution from the domain walls is expected to be solely due to the stationary domain wall contributions (not motional extrinsic contributions), which presents a unique opportunity to study the stationary response of domain walls to external stimuli quantitatively.

2.4 Conclusions

In this chapter, we have revealed that we are able to grow single phase epitaxial $PbZr_{0.2}Ti_{0.8}O_3$ films on different oriented substrates. This work reveals that in addition to the use of epitaxial strain [50], film thickness [42], and film composition [51] to manipulate domain structures in ferroelectrics, film orientation is another effective route by which to control the domain structure and domain wall density. In fact, (111)-oriented films enable the study of domain structures and densities not possible in other orientations at these film thicknesses. This enhanced density of domain walls will boost the contribution of such features to the overall response to applied stimuli. Furthermore, due to the degeneracy of the different domain variants the extrinsic contribution from the domain walls is expected to be solely due to

the stationary domain wall contributions (not motional extrinsic contributions), which presents a unique opportunity to study the stationary response of domain walls to external stimuli quantitatively.

CHAPTER 3

LOW FIELD DIELECTRIC PROPERTIES OF (001)-, (101)-, AND (111)-ORIENTED PZT THIN FILMS

Domain walls play an important role in determining the response of ferroelectrics to applied stimuli. While contributions to ferroelectric properties from the intrinsic response of the polarization within a domain and so-called extrinsic contributions from the motion of domain walls have been studied, the non-motional or stationary contribution from the material within the finite width of the domain wall itself has been particularly difficult to understand. In this chapter, we use a combination of phenomenological models, thin-film growth, and multi-scale characterization to probe model versions of (001)-, (101)-, and (111)-oriented epitaxial films. Here we report the direct measurement of the stationary domain wall contribution to dielectric susceptibility in nanodomain $PbZr_{0.2}Ti_{0.8}O_3$ thin films. In particular, we observe that (111)-oriented films, in which the extrinsic contributions from the high density of 90° domain walls are frozen out, exhibit permittivity values ~3-times larger than that expected from the intrinsic response alone. This discrepancy can only be accounted for by considering a stationary contribution to the permittivity from the domain wall volume of the material that is 6-77.5-times larger than the bulk response and is consistent with recent predictions of the enhancement of susceptibilities within 90° domain walls. This work offers new insights into the microscopic origin of dielectric enhancement and provides a pathway to engineer the dielectric response of these materials.

3.1 GLD Modeling of Polydomain Ferroelectric Thin Films

In order to study the intrinsic and motional extrinsic contributions to the dielectric permittivity, we considered thin films of the tetragonal ferroelectric $PbZr_{0.2}Ti_{0.8}O_3$ grown epitaxially on (001)-, (101)-, and (111)-oriented cubic substrates. We utilize the Helmholtz free energy formalism applicable to ferroelectric films with dense domain structures to calculate the domain structures and dielectric susceptibilities as a function of substrate orientation and epitaxial strain [52,53,35]. Consistent with prior approaches, we assume homogeneous strain fields within the domains and neglect the domain wall self-energies and inter-domain electrostatic interactions. Applying short-circuit electrical boundary conditions, the free energy of the system is minimized as a function of the in-plane strain imposed by the substrate so that we can calculate the equilibrium polarizations (P_1, P_2, P_3) and domain fractions. Using these models, we can then calculate explicitly the out-of-plane permittivity ($\varepsilon_\perp$) as the sum of the intrinsic (the first term) and the motional extrinsic (the second term) contributions [19, 52, 53, 54 as

$$\varepsilon_\perp = \sum_i \phi_i \cdot \left(\frac{d^2F}{d\left(P_i^\perp\right)^2}\right)^{-1} + \sum_i P_i^\perp \cdot \frac{d\phi_i}{dE} \quad (1)$$

(i = 1, 2, 3 corresponding to domains with polarization P_i)

where ϕ_i is the fraction of domains with polarization P_i, F is the free energy formalism, $P_i^\perp$ is the out-of-plane polarization component of P_i, and E is the electric field along the substrate normal. Note that these models exclude stationary domain wall contributions from the portion of the material contained within the finite width of the domain walls.

The domain volume fraction (ϕ) and dielectric permittivity ($\varepsilon_\perp$) have been calculated numerically for all three orientation variants as a function of misfit strain [Fig. 3.1]. For comparison, the strain regime that was explored was chosen to correspond to theoretically predicted epitaxial strains that give rise to *c/a/c/a* polydomain structures in (001)-oriented films [52,55]. In (001)-oriented films, the volume fraction of *c* domains (ϕ_{001}) is observed to decrease with increasing tensile strain, while the volume fraction of *a* domains (ϕ_{100} and ϕ_{010}) increases as a result of the tensile strain that favors in-plane oriented

polarization [Fig. 3.1 a]. A similar competitive trend is observed in (101)-oriented films where the population of the in-plane polarized domains (ϕ'_{010}) increases and the fraction of out-of-plane polarized domains (ϕ'_{100} and ϕ'_{001}) deceases with increasing strain [Fig. 3.1 b]. This is not the case for the (111)-oriented films, however, which due to symmetry, possess three energetically degenerate domain types and thus an equal volume fraction ($\phi''_{100} = \phi''_{010} = \phi''_{001} = 1/3$) of each domain separated by 90° domain walls at all values of misfit strain considered [Fig. 3.1 c]. Correspondingly, we can observe the impact of changing film orientation on $\varepsilon_\perp$ [Figs. 3.1 d-f]. In general, the intrinsic contribution to permittivity increases as the substrate normal is inclined more towards the [100] which is similar to the monodomain case where the permittivity exhibits higher values along non-polar directions (i.e., [111]) than polar directions (i.e., [001]) in tetragonal ferroelectrics [56,57]. This is due to the anisotropic dielectric response of $PbZr_{0.2}Ti_{0.8}O_3$ where the permittivity along the [100] is larger than that along the [001] [57]. Thus the enhanced intrinsic response in (101)- and (111)-oriented films arises from the fact that additional intrinsic contributions are activated. It is also noted that the increasing tensile strain results in an increasing

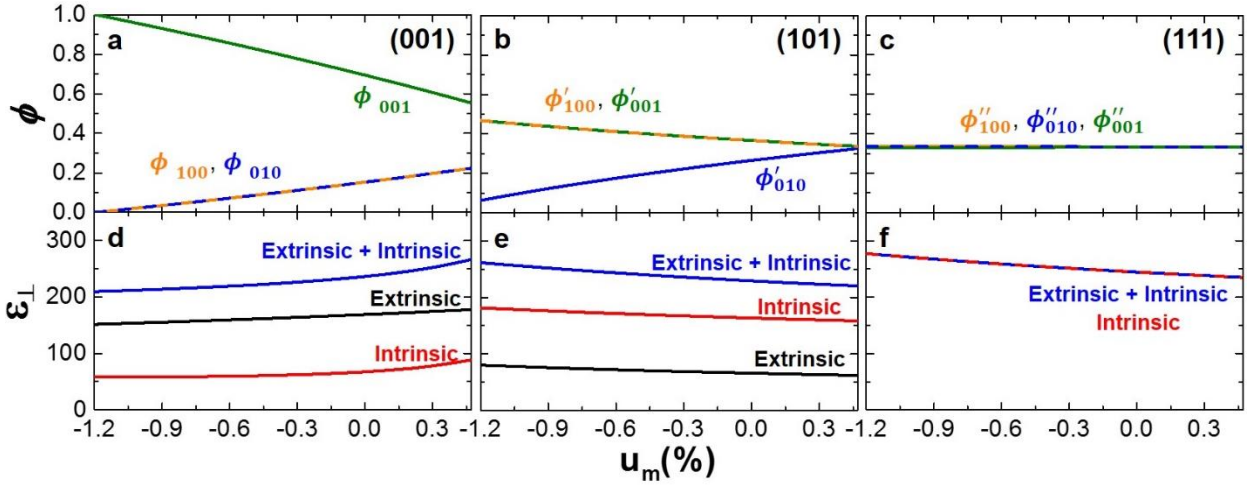

Figure 3.1: Using Ginzburg-Landau-Devonshire models, the volume fraction of polarization variants (ϕ) and out-of-plane, room temperature dielectric permittivity ($\varepsilon_\perp$) are predicted as a function of mismatch strain (u_m). The evolution of ϕ is provided for (a) (001)-, (b) (101)-, and (c) (111)-oriented films including the relative fraction of different polarization variants (referenced to the cardinal directions of the lattice, [100], [010], and [001]). The evolution of the intrinsic (red), extrinsic (black), and total (blue) $\varepsilon_\perp$ is provided for (d) (001)-, (e) (101)-, and (f) (111)-oriented films.

intrinsic response in the (001)-oriented films, which behaves in an opposite trend as compared to the (101)- and (111)-oriented films due to the fact that the intrinsic response of each polarization variant in (001)-oriented films increases while this component in (101)- and (111)-oriented films decreases with increasing tensile strain. At the same time, the relative contribution from the motional extrinsic response decreases as we move from (001)- to (101)-oriented films (as a result of less preferential alignment of the electric field with a single polarization variant) and completely vanishes in (111)-oriented films due to the constant volume fraction of the three polarization variants which is independent of the electric field. Similar to $BaTiO_3$ single crystals poled along [111] [58,59], the extrinsic contribution from domain wall motion will be "frozen out" in (111)-oriented PZT films. In addition, the motional extrinsic contribution $\left(\frac{d\phi_i}{dE}\right)$ for (001)- and (101)-oriented films behaves differently with increasing strain, leading to an increasing and decreasing extrinsic contribution in (001)- and (101)-oriented films, respectively. Despite these differences, across the entire strain regime studied here and for all three film orientations, the overall predicted $\varepsilon_\perp$ is found to exist in a rather narrow range between 220-290.

3.2 Low Field Dielectric Susceptibilities of PZT Thin Films

Detailed dielectric characterization of symmetric capacitor structures of the various orientations of films was performed. For all measurements reported herein, the capacitor structures were subjected to current-voltage and ferroelectric characterization first, including multiple switching processes to assess the nature of the hysteresis loops and to assure measurements of poled capacitors only. Only capacitors showing symmetric current-voltage response, well-saturated, symmetric, and imprint-free hysteresis loops across the frequency range 1 Hz – 10 kHz were probed [Fig. 3.2]. Frequency dependent polarization-electric field hysteresis loops were completed for at least 10 capacitors for the (001)-, (101)-, and (111)-oriented films [Fig. 3.2 a-c]. Measurements were completed on symmetric capacitor structures using $SrRuO_3$ or $La_{0.7}Sr_{0.3}MnO_3$ top and bottom electrodes. All films exhibit well saturated hysteresis loops with high remnant polarization and negligible imprint in the frequency range from 1-10,000 Hz. Furthermore, symmetric, low leakage currents are observed in all films as a result of the high quality insulating

ferroelectric and the symmetric electrode structure [Fig. 3.2 d]. In addition, low dielectric loss tangents (< 0.05) were measured for all film variants for much of the frequency range probed herein [Fig. 3.2 e].

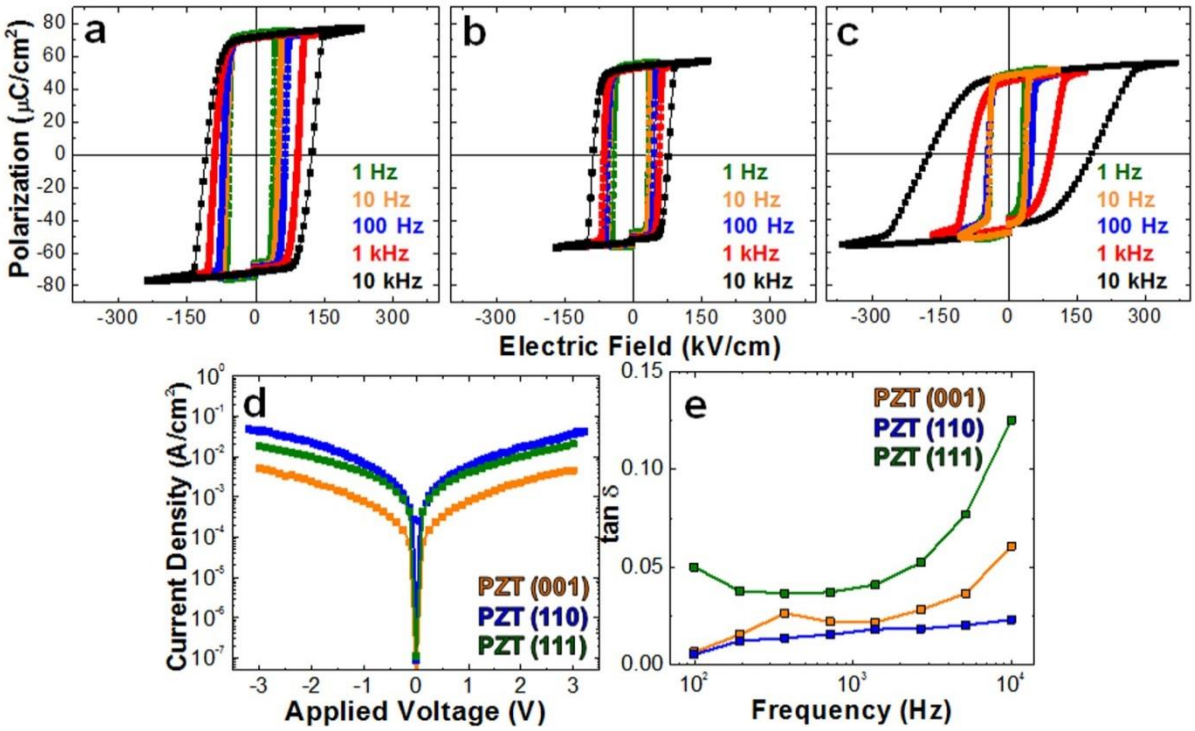

Fig. 3.2: Frequency dependent polarization-electric field hysteresis loops measured in (a) (001)-, (b) (101)-, and (c) (111)-oriented $PbZr_{0.2}Ti_{0.8}O_3$ films in the frequency range of 1 Hz to 10 kHz. (d) Leakage current – voltage and (e) loss tangents measured in the frequency range of 0.1 kHz – 10 kHz for (001)-, (101), and (111)-oriented $PbZr_{0.2}Ti_{0.8}O_3$ films.

Additionally, following the procedure described by Saito *et al.* [39], we can estimate values of polarization along the [001] by taking the remnant polarization (P_r) value and dividing by the fraction of domains which have an out-of-plane component of polarization and by the cosine of the angle between the polarization direction and the sample normal. This provides an estimate of the spontaneous polarization (P_s) along the [001] for each film orientation type. Here, we have reproduced the loops for all three orientations at 1 kHz [Fig. 3.3 a] to aid this discussion. From this data, we extract P_r values of 71, 52, and 44 μC cm^{-2} and P_S values (at 130 kV cm^{-1}) of 73, 56, and 47 μC cm^{-2} for (001)-, (101)-, and (111)-oriented films, respectively. Using the measured domain volume fractions (or domain wall density) for each sample, we again summarize the relative volume fractions of the minority and majority domains in each film orientation [Fig. 3.3 b]. This, in turn, allows us to estimate the P_S along the [001] to be 84, 90,

and 79 μC cm^{-2} for the (001)-, (101)- and (111)-oriented films. Consistent with the work of Saito *et al.*, the estimated P_S values along [001] are approximately constant across the different film orientations.

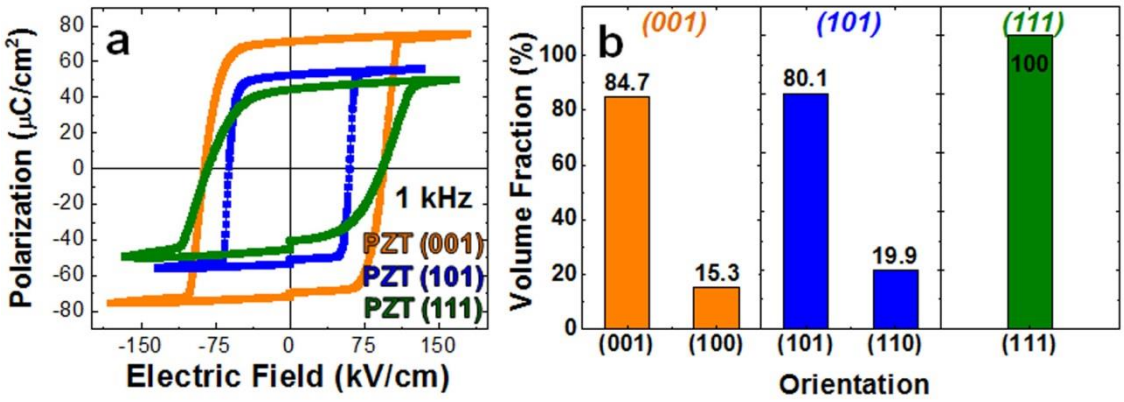

Figure 3.3: (a) Polarization-electric field hysteresis loops measured at 1 kHz and (b) Relative volume fraction of the majority and minority domains for $PbZr_{0.2}Ti_{0.8}O_3$ (001)-, (101)-, and (111)-oriented films.

The quality of the films and the accuracy of the measurements of domain wall density and domain fraction are confirmed using the procedure of Ref. [60] and the estimated values of polarization along the [001] are found to be approximately constant across the different orientations. Subsequently, the room temperature low-field dielectric permittivity ($\varepsilon_\perp$) was measured with an AC excitation field with an amplitude of 50 mV (in the frequency range from 0.1 kHz to 10 kHz). The (001)- and (101)-oriented films show values within the range $\varepsilon_\perp$= 185 – 267, while the (111)-oriented films exhibit significantly enhanced $\varepsilon_\perp$ = 654-691 across this same frequency range [Fig. 3.4].

A comparison of these measured values with the calculated permittivity from the GLD models was made by extracting the data point from Fig. 3.1 at the experimentally measured $\phi_{\min}$ given in Table 3.1. The calculated $\varepsilon_\perp$ (including both intrinsic and extrinsic contributions) for all three orientations shows small differences (all orientations are predicted to have values between 220–250), which agrees well with the experimental results for (001)- and (101)-oriented films. The (111)-oriented films, however, show a significant discrepancy between the experimentally measured and theoretically predicted values. As is noted in the discussion of the GLD model for the (111)-oriented films, all three degenerate polarization variants are present in equal volume fractions and these fractions will not vary with

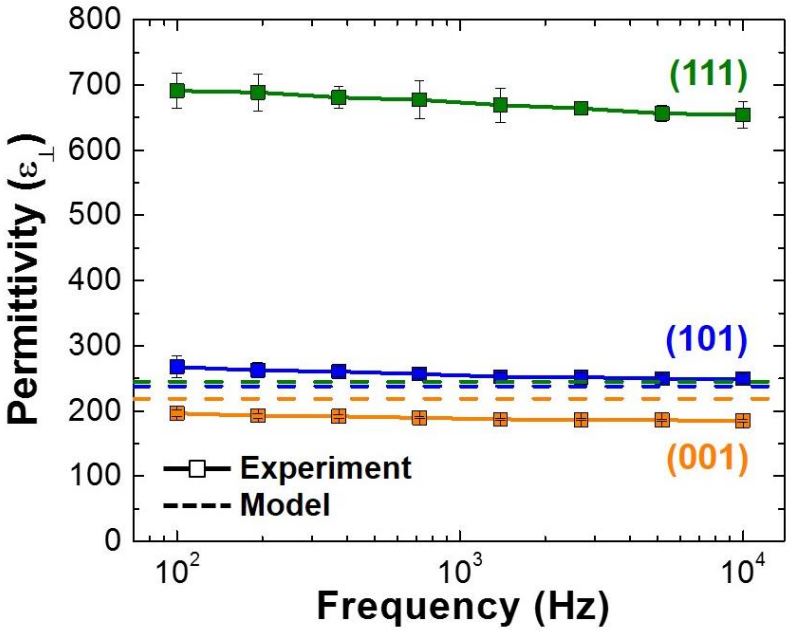

Figure 3.4: The solid symbol lines shows $\varepsilon_\perp$ measured at an AC excitation of 50 mV for (001)-, (101)-, and (111)-oriented $PbZr_{0.2}Ti_{0.8}O_3$ thin films. The dashed lines show the predicted $\varepsilon_\perp$ (including intrinsic and extrinsic contributions) from the Ginzburg-Landau-Devonshire models.

application of an electric field thus leading to an absence of a motional extrinsic contribution. The experimental results, however, imply that $\varepsilon_\perp$ for (111)-oriented films is greatly enhanced with increasing domain wall density (or decreasing average domain width). This enhancement suggests that the high density of domain walls in the (111)-oriented films could potentially give rise to a stationary domain wall contribution that can enhance the permittivity.

To further quantify this stationary domain wall contribution, we utilized an equivalent electrical circuit model to calculate the effective domain wall permittivity. Previous studies [44] suggest that the 90° domain walls present in the (111)-oriented heterostructures, by symmetry and to avoid charged domain boundaries, should be inclined from the plane of the film at an angle of ~33.9°. When applying electric field along the normal direction of the film, the electric field lines should proceed straight along the normal direction within the domains, but will be deflected from the vertical direction within the domain walls according to the Maxwell equation [Fig. 3.5]. Thus an appropriate model of an equivalent circuit for this system requires that we treat the domain and domain walls as capacitors in series where the effective

thickness of each capacitor is geometrically calculated based on the path-length of the field within that element. Using the experimentally measured average domain width (~40 nm), the experimentally measured $\varepsilon_{\perp}$ (~670), the calculated intrinsic dielectric permittivity (~245), and by assuming the domain wall width to be (conservatively) 1-10 nm [45-48,61] one can estimate ε_{dw} to be 1,500-19,000, which is 6-77.5 times larger than the expected intrinsic response within a domain. As noted above, recent theoretical work using a decoupling approximation and GLD modeling suggests the possibility of up to a thousand-fold enhancement of the dielectric susceptibility and piezoelectric response across 90° domains walls in tetragonal ferroelectrics (like those found in our samples) due to structural and polarization inhomogeneities within the domain wall region [24]. Our work, in turn, experimentally demonstrates that high density, stationary 90° domain walls could provide significantly enhanced dielectric response in the epitaxial thin films, particularly at large domain wall densities.

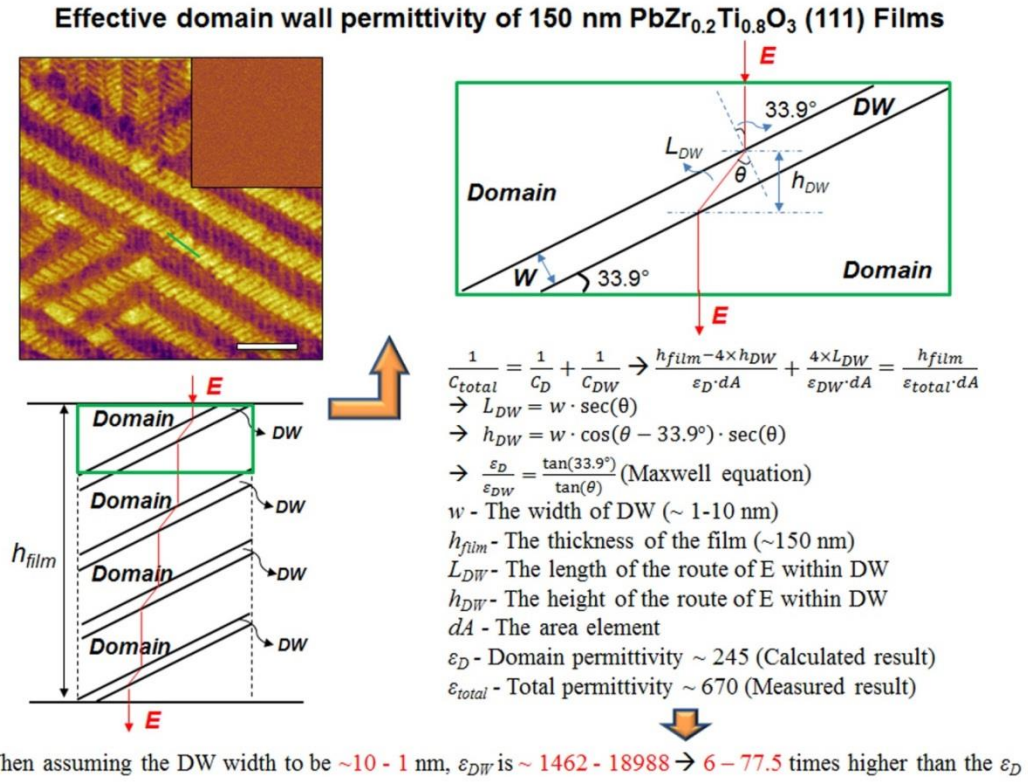

Figure 3.5: Detailed process of the extraction of the effective domain wall permittivity using an equivalent circuit approach. Scale bar: 500 nm.

3.3 Conclusions

The above results show that the application of electric field along certain non-polar directions in tetragonal ferroelectrics can be used to effectively "freeze out" the domain wall motion and thus enables us to probe the stationary domain wall contribution to susceptibility. This is aided by the fact that growth of (111)-oriented films produces a configuration of numerous degenerate polarization variants, enables the application of electric fields along non-polar directions, and produces domain wall densities high enough to promote the stationary domain wall contribution to be comparable in magnitude to the intrinsic response from the bulk of the domains. These observations, made possible by the simplicity of the engineered domain structure in the epitaxial thin films and our ability to directly probe the type, density, and response of these domain wall structures in different orientations produces a complimentary approach to the study ferroelectric single crystals with fields applied along different crystallographic directions and provides an opportunity to re-examine the importance of domain structure in controlling field-induced response.

These studies suggest that the stationary domain wall contribution to ferroelectric susceptibility should be given additional attention for its potential to enhance overall material performance. To date the understanding of intrinsic and motional extrinsic responses in these materials has led researchers to decrease the average domain size to enhance susceptibilities. The observed increase in performance, although likely partially enhanced by extra motional extrinsic contributions, could also be strengthened by simultaneous turn-on of stationary domain wall contributions. In one extreme case one could imagine that in systems controlled to have extremely fine domain structures, domain wall-domain wall interactions could lessen the extent of motional extrinsic contributions while still exhibiting enhancements in susceptibility from the stationary domain wall contribution. The failure to consider such stationary domain wall contributions, in turn, could result in the attribution of performance enhancements to the wrong feature in the material. Our work suggests that motional extrinsic contributions to permittivity are (at best) a factor of 2-times larger than the intrinsic response while stationary domain wall contributions

could be as large as 6-77.5 times larger than the intrinsic response [62,63]. This work provides a new intellectual framework in which to consider ferroelectric susceptibilities and to explain observations in a range of samples. Our observations provide new insights into the microscopic structural origin of enhanced ferroelectric susceptibilities and a new approach to optimize the properties of epitaxial thin films.

CHAPTER 4

HIGH FIELD SWITCHING PROPERTIES OF (001)-, (101)-, AND (111)-ORIENTED PZT THIN FILMS

Switchable polarization makes ferroelectrics a critical component in memories, actuators, and electro-optic devices and potential candidates for nanoelectronics. Although many studies of ferroelectric switching have been undertaken, much remains to be understood about switching in complex domain structures and in devices. In this chapter, a combination of thin-film epitaxy, macro- and nanoscale property and switching characterization, and molecular dynamics simulations are used to elucidate the nature of switching in $PbZr_{0.2}Ti_{0.8}O_3$ thin films. Differences are demonstrated between (001)-/(101)- and (111)-oriented films, with the latter exhibiting complex, nanotwinned ferroelectric domain structures with high densities of 90° domain walls and considerably broadened switching characteristics. Molecular dynamics simulations predict both 180° (for (001)-/(101)-oriented films) and 90° multi-step switching (for (111)-oriented films) and these processes are subsequently observed in stroboscopic piezoresponse force microscopy. These results have implications for our understanding of ferroelectric switching and offer opportunities to change domain reversal speed.

4.1 Macro-scale High Field Switching Properties of PZT Thin Films

We focus on 150 nm $PbZr_{0.2}Ti_{0.8}O_3$ / 10 nm $SrRuO_3$ or $La_{0.7}Sr_{0.3}MnO_3$ / $SrTiO_3$ (001), (110), and (111) heterostructures grown via pulsed-laser deposition. X-ray diffraction studies show that the films are epitaxial and single-phase [Fig. 4.1]. The ferroelectric domain structure was probed using PFM. Throughout the remainder of the discussion, we will use the following terminology to describe the polarization variants in the samples: for tetragonal $PbZr_{0.2}Ti_{0.8}O_3$, domains with polarization along the positive and negative [100], [010], and [001] axes will be referred to as $P_1^{+/-}$, $P_2^{+/-}$, and $P_3^{+/-}$, respectively. In (001)-oriented heterostructures, a typical polydomain structure with majority P_3^- domains and minority P_1^+ and P_2^- domains is observed [Fig. 4.2 a,b]. In (101)-oriented heterostructures, three different domain types are found [Fig. 4.2 c,d], with majority P_3^+ domains (in which the polarization is oriented at an angle of ≈43.6° from the plane of the film) and the remainder primarily composed of in-plane polarized stripe-like P_2^+ and P_2^- domains and small fractions of P_1^- domains (also oriented ≈43.6° from the plane of the film). The as-grown domain structure of the (001)- and (101)-oriented films, as probed by PFM studies which enable exact determination of the polarization directions, represents the equilibrium domain structure predicted for these film orientations, and does not change with electric field cycling [Fig. 4.3 a,b].

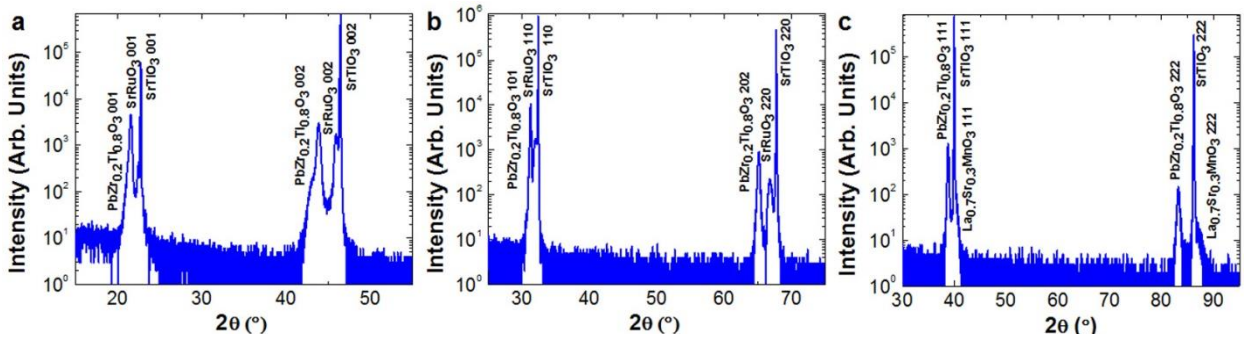

Figure 4.1: Crystal structure analysis. X-ray diffraction θ-2θ scans of (a) (001)-, (b) (101)-, and (c) (111)-oriented $PbZr_{0.2}Ti_{0.8}O_3$ films.

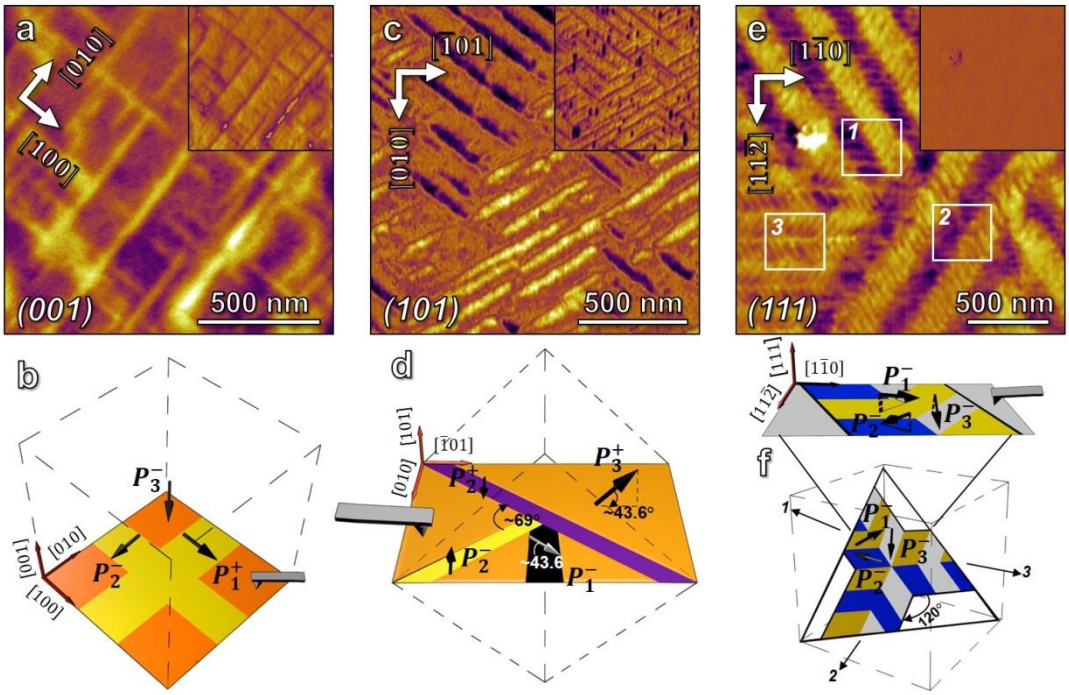

Figure 4.2: Lateral (*A*cosθ, combining phase θ and amplitude *A*) and vertical (*A*cosθ, inset) piezoresponse force microscopy images for equilibrium domain structures and corresponding illustrations of those domain structures for (a), (b) (001)-oriented heterostructures with majority P_3^- domains (orange domains) and minority P_1^+ and P_2^- domains (yellow domains); (c), (d) (101)-oriented heterostructures with majority P_3^+ domains (with polarization oriented at ≈43.6° from the plane-of-the-film, orange domains) and minority domains including stripe-like P_2^+ and P_2^- domains (in-plane polarized, purple domains) and small fractions of P_1^- domains (with polarization oriented at ≈43.6° from the plane-of-the-film, black domains); (e), (f) (111)-oriented heterostructures with complex nanotwinned domain structures wherein there are three degenerate polarization variants $P_1^-, P_2^-,$ and P_3^- oriented at an angle of ≈33.9° from the plane of the film (represented by yellow, blue, and grey domains, respectively) which are tiled to produce three degenerate domain bands separated by 120° as labeled in the open squares (1), (2), and (3).

Analysis of the (111)-oriented heterostructures reveals a dramatically different picture. The as-grown domain structure has a complex, metastable nanoscale domain pattern [Fig. 4.3 c,d]. A domain structure consistent with that predicted to the equilibrium domain structure is obtained after a series of ±6 V dc voltages were applied to the PFM tip to switch a 1.5 μm × 1.5 μm region of the film a total of 2-6 times. The domain pattern consists of a high density of nanotwinned domains [Fig. 4.2 e]. The observed domain structure is the result of the tiling of three types of domain bands, separated by 120° (noted as areas 1, 2, and 3, Fig. 4.2 e) with average domain band widths of ≈300 nm. Within each domain band, the domain structure consists of a mixture of all three degenerate polarization variants ($P_1^-, P_2^-,$ and P_3^-, each

possessing a polarization direction that is oriented at an angle of ≈33.9° form the plane of the film) distributed into two sub-bands, with each sub-band composed of only two of the polarization variants. The average domain size within the domain sub-bands is ≈40 nm. The geometry of such domain structures is shown in a schematic illustration [Fig. 4.2 f]. Prior theoretical treatments predicted such equilibrium domain structures [44].

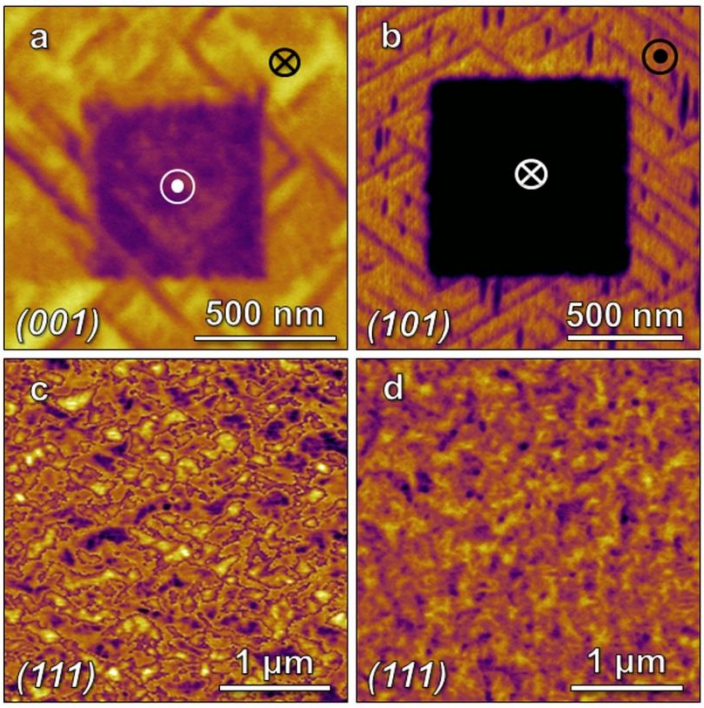

Figure 4.3: Vertical (*A*cosθ, combining phase θ and amplitude *A*) piezoresponse force microscopy images of $PbZr_{0.2}Ti_{0.8}O_3$ of (a) (001)-oriented films after applying a negative tip bias of -5 V in PFM to locally switch a central square region, which indicates the as-grown down-poled domain structure, (b) (101)-oriented films after applying a positive tip bias of 4 V in PFM to locally switch a central square region, which indicates the as-grown up-poled domain structure. (c) Vertical (*A*cosθ, combining phase *θ* and amplitude *A*) and (d) lateral (*A*cosθ, combining phase *θ* and amplitude *A*) piezoresponse force microscopy images of the as-grown domain structure in (111)-oriented films showing a complex metastable nanoscale domain pattern.

Having established the difference in domain structures for the various heterostructure orientations, we probed their dielectric and ferroelectric properties using symmetric metal-oxide capacitor structures [64] and MD simulations. All heterostructures, regardless of orientation, were found to exhibit symmetric, well-saturated polarization-electric field hysteresis loops [Fig. 4.4 a] that are maintained down to at least 1 Hz. As expected, the saturation polarization scales with the film orientation, with (001)- and (111)-oriented films having the largest and smallest values, respectively. In addition, although all films possess high remnant polarization, the (001)- and (101)-oriented films show nearly square hysteresis loops with sharp electric field switching, while (111)-oriented films exhibit more slanted hysteresis loops regardless of frequency, indicative of switching at a broader range of fields.

The dielectric permittivity was then measured as a function of increasing ac electric field excitation. Since we are focused here on switching behavior, we have extended this analysis to larger fields than are typically applied in Rayleigh studies. These studies reveal that (111)-oriented heterostructures exhibit a lower threshold field (8.2 kV/cm) for the onset of non-linearity (or polarization switching) as compared to (001)- and (101)-oriented films (46.3 kV/cm and 22.5 kV/cm, respectively) [Fig. 4.4 b]. Additionally, the field dependence of the dielectric response of the (111)-oriented film shows a gradual increase (and, therefore, ferroelectric switching) over a much larger range of fields, relative to the (001)- and (101)-oriented films, consistent with the polarization-electric field hysteresis loops [Fig. 4.4 a].

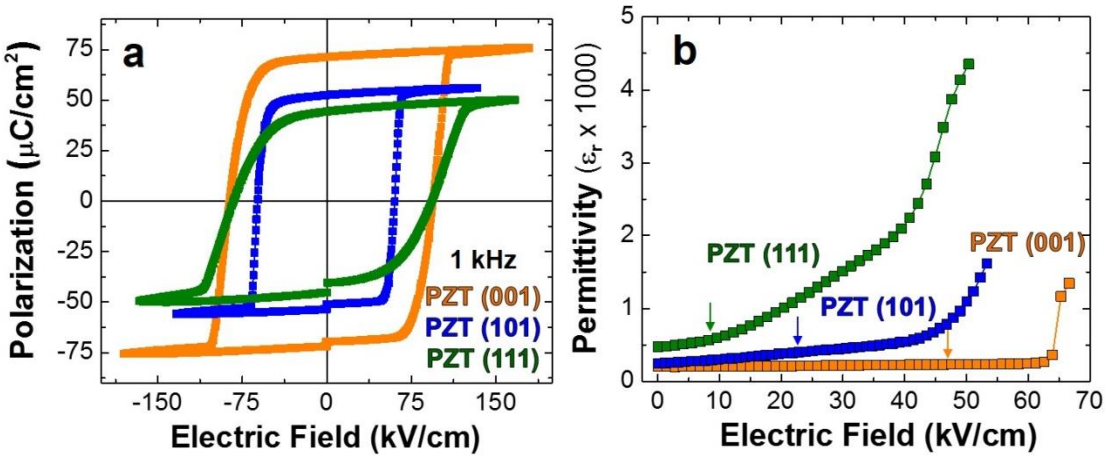

Fig. 4.4: (a) Polarization - electric field hysteresis loops measured at 1 kHz and (b) permittivity as a function of ac electric field measured at 1 kHz for (001)-, (101)-, and (111)-oriented $PbZr_{0.2}Ti_{0.8}O_3$ thin films. The arrows demarcate the location of the onset of non-linearity from the Rayleigh studies.

4.2 Molecular Dynamics Simulations of Switching Properties of PZT Thin Films

To understand what gives rise to these different electric field responses, we used MD simulations to examine the evolution of domain switching under differently oriented electric fields. We studied the evolution of domain structures resembling those experimentally observed in (001)-, (101)- and (111)-oriented films possessing 90° domain walls under electric fields applied along the film normal directions

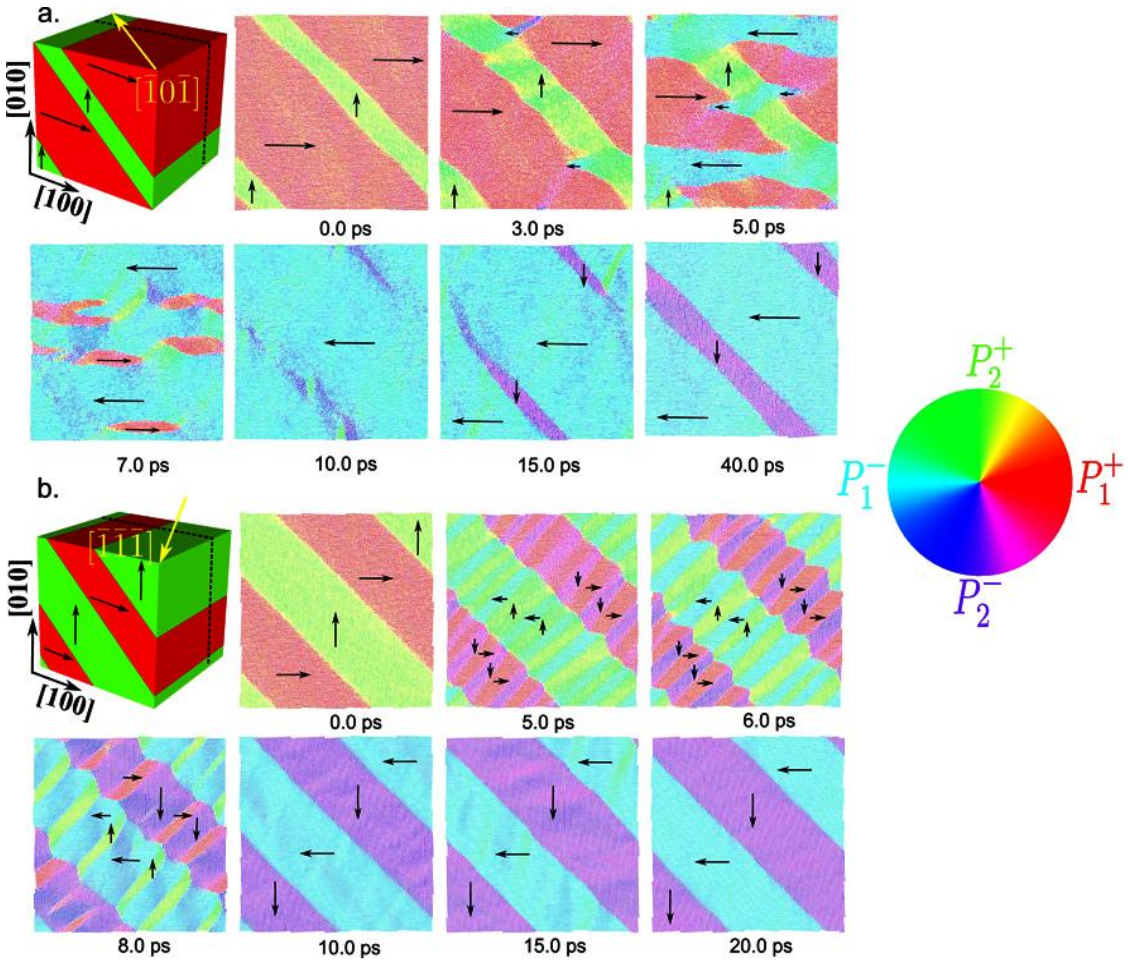

Figure 4.5: Molecular dynamics simulations of switching in domain structures possessing 90° domain walls. These images show the evolution of domain structures under applied field. In both cases, the electric field is turn-on at 0.0 ps and off at 10 ps and allowed to relax at zero applied field from that point. The colors in the domain maps correspond to the polarization wheel shown at the right. (a) This simulation focuses on a domain structure that would be found in a (101)-oriented film. The domain structure consists of 20 volume % of minority (green, P_2^+) domains with polarization along [010] and 80 volume % of majority (red, P_1^+) domains with polarization along [100]. The electric field is applied along the $[\bar{1}0\bar{1}]$ (yellow arrow) to the initial domain structure. As the domains evolve, direct 180º reversal is observed ($P_2^+ \rightarrow P_2^-$ and $P_1^+ \rightarrow P_1^-$). (b) This simulation focuses on a domain structure that would be found in a (111)-oriented film. The domain structure consists of 50 volume % domains (green, P_2^+) with polarization along [010] and 50 volume % of domains (red, P_1^+) with polarization along [100]. The electric field is applied along the $[\bar{1}\bar{1}\bar{1}]$ (yellow arrow) to the initial domain structure. During the application of the field, 90º switching events ($P_2^+ \rightarrow P_1^-$ and $P_1^+ \rightarrow P_2^-$) are observed. The local polarization within each unit cell is represented with an arrow that is colored based on the angle formed with [100] axis.

$[00\bar{1}]$, $[\bar{1}0\bar{1}]$ [Fig. 4.5a], and $[\bar{1}\bar{1}\bar{1}]$ [Fig. 4.5b], respectively. The volume fraction of the minority domain used in the simulations is based on experimental observations. The MD simulations provide a time-resolved view of the evolution of the domain structure including specific polarization variants [Fig. 4.6].

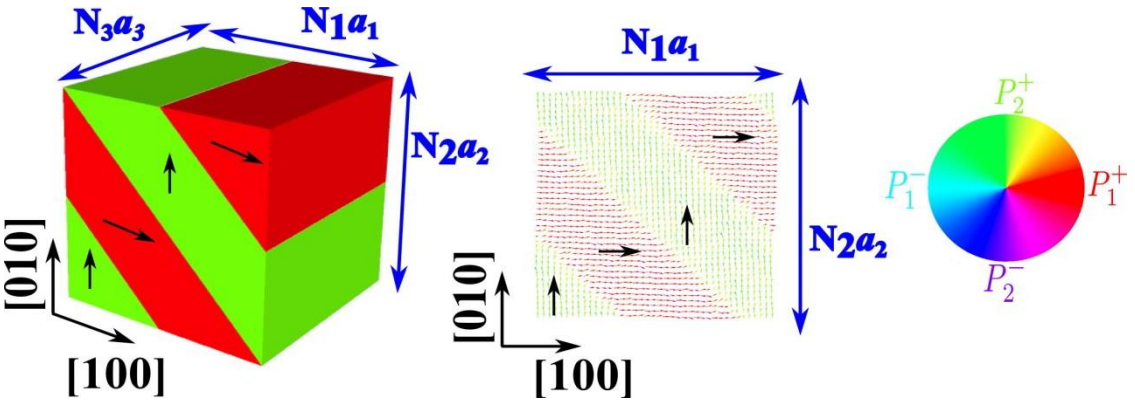

Figure 4.6: Molecular dynamics simulations. (a) Domain structures possessing 90° domain walls constructed with a 40×40×40 supercell, (b) zig-zag domain patterns in {001} plane. $\gamma =$ 0.5.

For brevity, we discuss here only the detailed MD studies of (101)-oriented films. In the case of (101)-oriented films, in the initial state (0.0 ps) we simulate a domain configuration with 20% minority P_2^+ domains (green, Fig. 4.5 a) and 80% majority P_1^+ domains (red, Fig. 4.5 a) with the electric field applied along the $[\bar{1}0\bar{1}]$ (yellow arrow, Fig. 4.5 a). This results in a series of complicated changes [Fig. 4.5 a]. At 3 ps, we observe that the volume fraction of P_2^+ domains increases as they widen via changes of the type $P_1^+ \rightarrow P_2^+$ at the domain boundary due to the $[\bar{1}00]$-component of the electric field. In addition, a significant number of P_1^+ dipoles close to domain boundaries are switched by 180° to P_1^- dipoles (cyan). Further application of electric field facilitates the growth of the P_1^- domains via the 180° switching process of $P_1^+ \rightarrow P_1^-$ (see 5 and 7 ps images, Fig. 4.5 a). At 10 ps, the whole supercell reaches a nearly single-domain state. Subsequent relaxation of the structure (after the field is turned off) for another 30 ps results in the reemergence of domain structures similar to that in the initial state (albeit poled in the opposite direction) due to strain accommodation. The lateral shift of the domain boundary is likely due to the application of large electric field to achieve picosecond switching in MD simulations.

In the case of (111)-oriented films, in the initial state (0.0 ps) we simulate a domain configuration with 50% P_1^+ domains (red, Fig. 4.5 b) and 50% P_2^+ domains (green, Fig. 4.5 b) with the electric field applied along the $[\bar{1}\bar{1}\bar{1}]$ (yellow arrow, Fig. 4.5 b). This process results in a fundamentally different

domain switching evolution [Fig. 4.5 b]. First, we observe that there is no significant domain wall motion. Although decidedly different from the behavior in (101)-oriented films, this is expected since all polarization directions are energetically equivalent with respect to the applied field. Additionally, at 5 ps, we see new domains perpendicular to their parent domains appear via two types of 90° switching processes: $P_1^+ \rightarrow P_2^-$ and $P_2^+ \rightarrow P_1^-$, respectively. By 8 ps, the new domains spread quickly across their parent domains and dipole frustration at domain boundaries, leading to transient charged domain walls, is also observed. This switching process continues, until the final configuration of P_1^- and P_2^- domains is achieved by 10 ps. The strain-driven structural relaxation for another 10 ps in the absence of electric field leads to a slight change in the positions of domain walls, but overall the reemergence of domain structures similar to that in the initial state (albeit poled in the opposite direction).

4.3 PFM Analysis of Local-Scale Switching Characteristics

What these MD simulations reveal, is that if one only considers the starting and final states, the domain structures could potentially lead one to assume only 180° switching has taken place on the macroscale. These time-dependent models, however, reveal a more nuanced evolution with clear differences between (001)-/(101)- and (111)-oriented films with the latter revealing a multi-step, 90° switching domain reversal process. To further explore these proposed switching pathways and their implications for material properties, we completed local-scale PFM switching studies where a time series of images was produced while incrementally increasing the applied tip bias. Focusing first on switching in the (001)- and (101)-oriented films, similarly abrupt switching processes occurring in a narrow field range have been observed, consistent with the macroscale property studies. For brevity, we discuss here only the detailed switching studies of (101)-oriented films [Fig. 4.7]. The (101)-oriented films show no obvious contrast change in either the lateral or vertical PFM images [Fig. 4.7 a, b] when applying biases from 0-3.0 V to locally switch a 1 μm × 1 μm square region in the center of the scanned area. A schematic of this domain structure before switching is provided [Fig. 4.7 c]. Upon increasing the applied tip bias further, to 3.5 V, domains in the film start to switch, resulting in a contrast change in both the lateral and

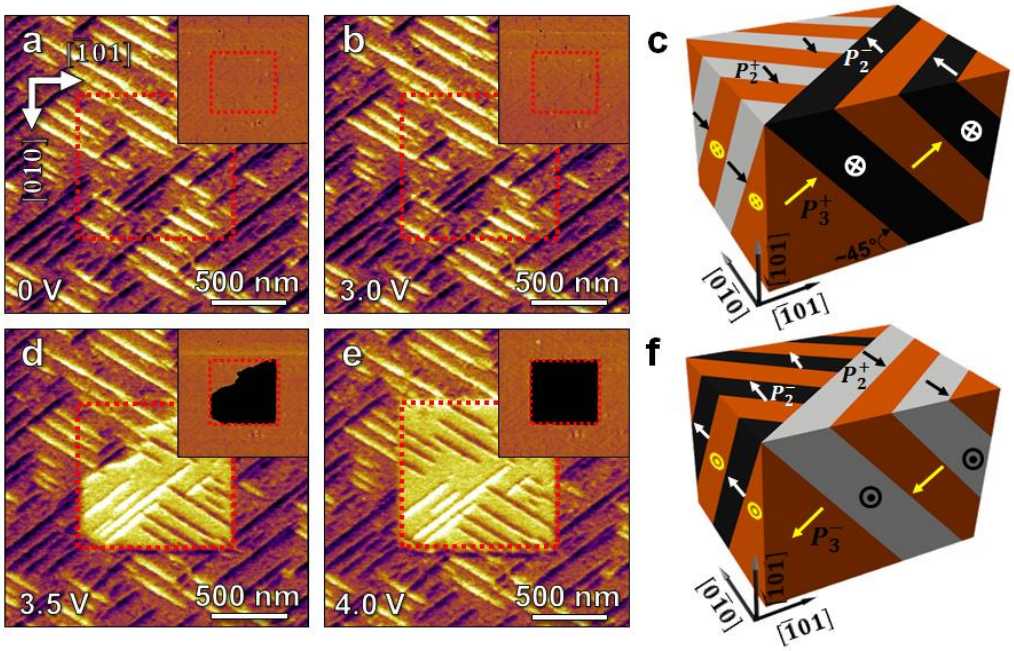

Figure 4.7: Piezoresponse force microscopy switching studies of $PbZr_{0.2}Ti_{0.8}O_3$ (101) thin films. Lateral (Acosθ, combining phase θ and amplitude A) and vertical (phase θ, inset) piezoresponse force microscopy images of field-dependent domain structure evolution in (101)-oriented $PbZr_{0.2}Ti_{0.8}O_3$ in the (a) as-grown state and (b) after applying a tip bias of 3.0 V in the central square region. (c) Schematic illustration of the observed, unswitched domain structure with the majority P_3^+ (orange domains, oriented at an angle of 43.6° from the plane of the film) and the stripe-like P_2^- (black domains) and P_2^+ (white domains) domains (in-plane polarized). Upon increasing the applied tip bias to (d) 3.5 V and (e) 4.0 V, abrupt switching is observed. (f) Schematic illustration of the switched domain structure in (d) and (e) with the majority P_3^- (orange domains), P_2^- (black domains), and P_2^+ (white domains) after the 180° switching

vertical PFM images [Fig. 4.7 d]. Further increasing the bias to 4.0 V results in complete switching of the central square region [Fig. 4.7 e]. Based on the PFM images, the final switched domain structure is interpreted such that both domains initially possessing polarization P_3^+(orange regions, Fig. 4.7 c) and in-plane oriented stripe domains P_2^- and P_2^+ (black and grey regions, Fig. 4.7 c) are switched by 180° [Fig. 4.7 f]. These observations are consistent with the abrupt switching that occurs in a narrow field range in the polarization hysteresis loops and with the abrupt increase of dielectric response in the Rayleigh analysis. These results indicate that 180° switching reversal occurs in (101)-oriented films, in agreement with MD prediction.

Similar studies of (111)-oriented films, however, reveal decidedly different responses with a complex evolution of domain structures involving four characteristic steps in the switching [Fig. 4.8 a-d].

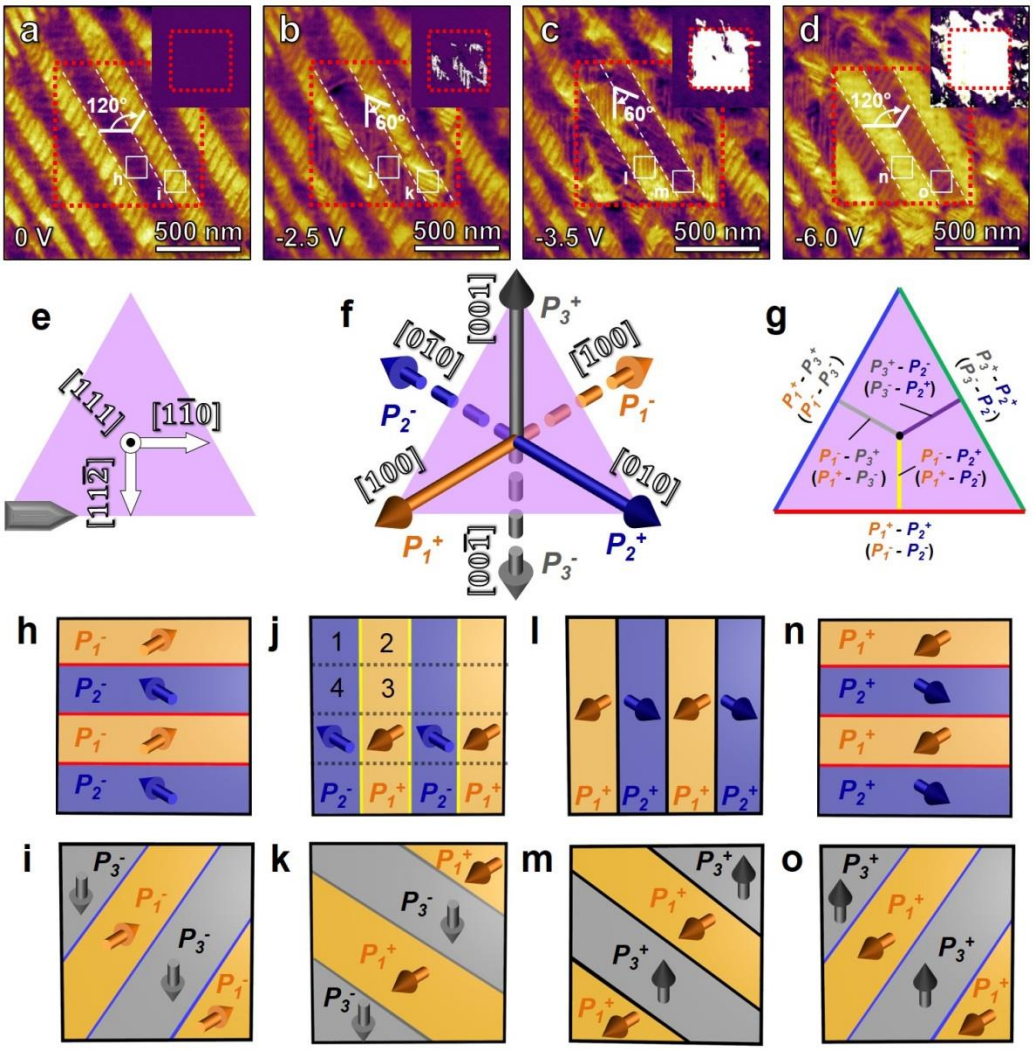

Figure 4.8: Piezoresponse force microscopy switching studies of $PbZr_{0.2}Ti_{0.8}O_3$ (111) thin films. Lateral ($A\cos\theta$, combining phase θ and amplitude A) and vertical (phase θ, inset) piezoresponse force microscopy images of field dependent domain structure evolution in (111)-oriented $PbZr_{0.2}Ti_{0.8}O_3$ in the (a) initial down-poled state, after applying a tip bias of (b) -2.5 V to achieve partial switching, (c) -3.5 V to achieve complete out-of-plane switching, but incomplete in-plane switching, and (d) -6.0 V to achieve complete out-of-plane and in-plane switching. Schematic illustrations of the geometry of the sample are provided including (e) the projection of the crystallographic axes, (f) the six possible polarization variants (solid pointing out of the plane and dashed pointing into the plane of the film), and (g) the six possible distinct 90° domain boundaries (each given a unique color that is carried throughout the remaining panels). Additional illustrations of the proposed switching process for dark and light domain bands, respectively, for the (h) and (i) initial state, (j) and (k) a majority down-poled intermediate state, (l) and (m) an up-poled intermediate, and (n) and (o) the final, fully switched state.

Detailed static domain structure characterization of the (111)-oriented films has been discussed above, and here we focus on an area possessing fully down-poled nanotwinned domain bands of a single type for simplicity [Fig. 4.8 a]. When applying a tip bias of –2.5 V to locally switch a 1 μm × 1 μm square region,

only a small fraction of the domains switch [inset, Fig. 4.8 b]. Examination of the lateral PFM contrast reveals that the orientation of the long axes of the domains that were switched rotates by 90° in-the-plane of the film, resulting in a new domain configuration with a characteristic angle of 60° between the domain sub-bands [Fig. 4.8 b]. Upon further increasing the bias to –3.5 V, the majority of the square region subjected to the bias has been switched in the out-of-plane direction [inset, Fig. 4.8 c] with the contrast changing accordingly in the lateral PFM images to reveal a characteristic angle of 60° between all domain sub-bands in the switched region [Fig. 4.8 c]. The domain structure does not exhibit further evolution until the applied tip bias exceeds –6 V. At this point, all domains in the square region subjected to the bias have been fully up-poled [inset, Fig. 4.8 d]. The nanotwinned domain pattern is observed to return to the initial orientation and reestablishes the characteristic angle of 120° between the long axes of the domains [Fig. 4.8 d]. Although a similar nanotwinned domain structure has been achieved, the in-plane contrast in the nanotwinned array has changed as compared to the initial state (*i.e.*, sub-bands with dark PFM contrast become light and vice versa, Fig. 4.8 d) suggesting that full switching is accompanied by an orientation change of the in-plane component of polarization.

This multi-step switching process is intriguing, and here we systematically analyze it. We provide schematic illustrations of the geometry of the sample including the crystallographic axes [Fig. 4.8 e], the six possible polarization variants [Fig. 4.8 f], and the twelve possible (six distinct) 90° domain boundaries (*i.e.*, those between $P_1^+ - P_2^+$ ($P_1^- - P_2^-$), $P_1^+ - P_3^+$ ($P_1^- - P_3^-$), $P_2^+ - P_3^+$ ($P_2^- - P_3^-$), $P_1^+ - P_2^-$ ($P_1^- - P_2^+$), $P_1^+ - P_3^-$ ($P_1^- - P_3^+$), $P_2^+ - P_3^-$ ($P_2^- - P_3^+$); each given a unique color in the figure) [Fig. 4.8 g] projected on the (111) of the PFM image. To aid the discussion, we provide schematic illustrations of the domain structures [Fig. 4.8 h-o] in each distinct domain sub-band type for the four PFM images [Fig. 4.8 a-d]. Three different colors (orange, blue, and grey) are used to represent the three different polarization variants with solid and dashed lines corresponding to down- and up-poled versions, respectively. In the initial state (Fig. 4.8 a), all domains are down-poled, and the dark [Fig. 4.8 h] and light [Fig. 4.8 i] domain sub-bands consist of alternating P_1^-/P_2^- and P_1^-/P_3^- domains, respectively. Upon application of the –2.5 V applied bias [Fig. 4.8 b], the orientation of the domain boundaries in both the dark [Fig. 4.8 j] and light

[Fig. 4.8 k] domain sub-bands are found to rotate by 90° in-the-plane of the film. Such a change in the domain boundary orientation can only be achieved by a complex switching process which includes three different switching events including 90° switching that maintains the vertical component of the polarization ($P_1^- \rightarrow P_2^-$, area 1, Fig. 4.8 j), 180° switching ($P_1^- \rightarrow P_1^+$, area 2, Fig. 4.8 j), and 90° switching that changes the vertical component of the polarization ($P_2^- \rightarrow P_1^+$, area 3, Fig. 4.8 j) as well as regions that experience no switching ($P_2^- \rightarrow P_2^-$, area 4, Fig. 4.8 j). Similar complex switching occurs in the light domain sub-bands as well [Fig. 4.8 k]. Upon further increasing the bias to –3.5 V [Fig. 4.8 c], the orientation of the domain boundaries remains the same, but all domains are now up-poled [Fig. 4.8 l,m] with a change of the in-plane contrast from light to dark (and vice versa) for the different domain sub-band types. This switching process includes 90° switching that maintains the vertical component of the polarization ($P_1^+ \rightarrow P_2^+$, Fig. 4.8 l) and 90° switching that changes it ($P_2^- \rightarrow P_1^+$, Fig. 4.8 l). Similar 90° switching events occur in the other domain sub-bands [Fig. 4.8 m]. Based on the PFM analysis, this up-poled domain structure should likely possess charged domain walls; however, it is not changed until the applied bias is further increased to –6 V [Fig. 4.8 d]. At this point, the domain boundaries are again rotated in-the-plane of the film by 90° and the domain structure is returned to a configuration consistent with the initial state [Fig. 4.8 n,o], but with a change of the in-plane contrast in the PFM from light to dark (and vice versa) for the different domain sub-band types. Again, the domain walls in the final state are uncharged. This process is again accomplished by two types of 90° switching events that maintain the vertical component of the polarization ($P_1^+ \rightarrow P_2^+$ and $P_2^+ \rightarrow P_1^+$, Fig. 4.8 n). Again, similar 90° switching events are observed for both domain sub-band types [Fig. 4.8 o]. Overall, what is observed is that regardless of the way the material is probed, be it MD simulations, macroscopic excitation of capacitor structures, or local excitation at scanning-probe tips (all of which could potentially provide for slight differences in the nature of the excitation profile and the final domain structure produced), we observe that the governing mechanism for switching remains the same. (001)-/(101)-oriented films switch via 180° switching processes while (111)-oriented films undergo domain reorientation via 90° switching mediated processes.

Although the nucleation and growth process for 180° switching events is fairly well understood, little evidence for 90° switching mediated domain reversal has been presented. It has been suggested that broadened (or double) current peaks during reverse switching of previously poled $PbZr_{0.415}Ti_{0.585}O_3$ ceramics could be the result of non-180° domain switching as a result of the residual stresses developed during forward poling [65] and that in single-crystals of [111]-oriented 95.5% $PbZn_{1/3}Nb_{2/3}O_3$ – 4.5% $PbTiO_3$, polarization reversal through intermediate polarization rotations of 71° and 109° can occur [66,67]. Despite these observations, the mechanisms underlying such behavior are not entirely clear [68] and no direct measurements and examples of 90° switching mediated domain reversal have been reported in the literature. This is particularly the case for thin films where there are no reports in this regard. In thin films, the 90° domain switching process, due to the elastic clamping of the substrate, is thought to be so energetically costly that it does not typically occur. Enhanced 90° domain switching can be realized in thin films if the effect of clamping can be compensated by engineering specific film or domain structures such as in patterned ferroelectric layers [69] or through a layered structure where the top layer is anchored on an underneath layer of a secondary ferroelectric phase [70]. Here we have achieved the 90° switching mediated domain reversal process in thin films by utilizing (111)-oriented domain structures where the energetics are such that it permits these events to take place.

The preference for a 90° or 180° switching process in different films is ultimately controlled by the clamping of the ferroelectric film (and the resulting domain size). In both (001)-/(101)-oriented heterostructures, the elastic constraints from the substrate lead to dramatic differences in the fraction of in-plane and out-of-plane polarized domains (in particular, minimizing the fraction of in-plane polarized domains). Although 90° domain walls have lower domain wall energy than 180° domain walls [71], the 90° ferroelastic switching in thin films is generally unfavorable as compared to the 180° ferroelectric switching (as we observed for (001)-/(101)-oriented films in our simulations) under moderate electric fields because of the large energy penalty associated with the change of volume fractions of in-plane and out-of-plane polarized domains that must occur to accommodate such switching events [72]. Said another way, the free energy change (Δf) for a ferroelastic 90° switching event is dominated by the contributions

from the stress (σ^2) and the stress-polarization coupling (σP^2) terms. These energy terms are high in the (001)-/(101)-oriented films due to the elastic constraints of the substrate and the drastically different stress states for an in-plane or out-of-plane polarized domain. On the other hand, the (111)-oriented films possess three energetically-degenerate polarization variants (in a fully-poled state) all possessing in-plane and out-of-plane polarization components that are the same and, in effect, renders the elastic energy costs associated with a ferroelastic 90° switching event greatly reduced. Additionally, our MD simulations reveal that coordinated 90° switching events (*i.e.*, $P_1^+ \rightarrow P_2^-$ and $P_2^+ \rightarrow P_1^-$) occur in essentially equal proportions across the entire domain width to accommodate (and maintain) both the elastic and electrostatic energy state of the system. As a result, the coordinated, multi-step 90° switching process will not incur a large elastic energy cost in agreement with the arguments above. Ultimately the preference of the 90° switching over the 180° switching in the (111)-oriented films is due to the lower kinetic barrier for 90° polarization rotation indicated by the lower energy of the 90° domain wall compared to that of the 180° domain wall.

The observation of such 90° switching mediated domain reversal, in turn, has important implications for our overall understanding of ferroelectric materials and their utilization in devices. First, the presence of active intermediate switching states can be correlated to the differences observed in the dielectric and ferroelectric response of the various orientations of films. Although all films possess high remnant polarization, the (001)-/(101)-oriented films show nearly square hysteresis loops with sharp electric field switching (consistent with 180° switching events), while (111)-oriented films exhibit more slanted hysteresis loops with larger coercive fields, indicative of switching at a broader range of fields and a multi-step switching process. Furthermore, it is likely that the availability of low-field intermediate switching can account for the observation of lower threshold fields for the nucleation of switching events in the Rayleigh studies of the (111)-oriented films. The domain reversal process is significantly impacted by changing the orientation of the epitaxial film and by allowing all possible switching types to be active in the material. Ultimately, if we can create pathways similar to those demonstrated in the stroboscopic PFM studies by which to deterministically stabilize or incrementally step the switched polarization from

one state, through a number of intermediate states, before reaching the oppositely poled state, the possibility for creating new modalities of low-power, multi-state memory or logic are possible. At the same time, if we can determine ways to promote the 90° switching mediated domain reversal process, this could further accelerate the domain reversal and reduce the timescale of ferroelectrics thereby increasing their potential for use in advanced nanoelectronics.

4.4 Conclusions

In conclusion, we have observed both 180° and multi-step 90° switching domain reversal processes in $PbZr_{0.2}Ti_{0.8}O_3$ thin films. Using a combination of epitaxial thin-film growth, macro- and nano-scale characterization, and MD simulations, we have been able to manipulate the domain structure through the control of film orientations and explore the coupling between the domain structures and properties. Specifically, stark differences between (001)-/(101)- and (111)-oriented films were observed, with the latter exhibiting complex, nanotwinned ferroelectric domain structures with high densities of 90° domain walls, considerably broadened ferroelectric switching characteristics, and lower threshold fields for the onset of non-linearity during Rayleigh studies. Subsequent MD simulations and PFM studies reveal both types of switching mechanisms are possible, but that the switching process that ultimately occurs is determined by a combination of factors including domain wall energy, elastic strain, and domain size. These observations provide insight into a previously unexplored aspect of ferroelectric switching and highlight the complexity of these materials. Such studies are crucial for developing precise control of nanoscale ferroelectric materials and can potentially lead to interesting multi-state devices and accelerated switching in ferroelectrics.

CHAPTER 5

SUMMARY AND SUGGESTIONS FOR FUTURE WORK

5.1 Summary of Findings

In this thesis, we have systematically studied the effects of film orientations on low field dielectric susceptibilities and high field switching characteristics in $PbZr_{0.2}Ti_{0.8}O_3$ thin films. The present work has developed new theoretical tools that combined orientation effects into the conventional GLD modeling that allows a more comprehensive model which could consider the effects of film orientation, epitaxial strain, and film composition. Here we use a combination of theoretical approaches (phenomenological Ginzburg-Landau-Devonshire model and Molecular Dynamics modeling) and experiment (thin film epitaxial and nanoscale domain structure and property characterization) to investigate the effects of film orientation on low field dielectric susceptibilities and high field switching characteristics in $PbZr_{0.2}Ti_{0.8}O_3$ thin films. We find that that varying the film orientation can dramatically manipulate the domain structure and domain wall density. In particular, we observe that (111)-oriented films, in which the extrinsic contributions from the high density of 90° domain walls are frozen out, exhibit permittivity values approximately 3-times larger than that expected from the intrinsic response alone. This discrepancy can only be accounted for by considering a stationary contribution to the permittivity from the domain wall volume of the material that is 6-77.5-times larger than the bulk response and is consistent with recent predictions of the enhancement of susceptibilities within 90° domain walls. In addition, differences are also demonstrated between (001)-/(101)- and (111)-oriented films, with the latter exhibiting complex, nanotwinned ferroelectric domain structures with high densities of 90° domain walls and considerably broadened switching characteristics. Molecular dynamics simulations predict both 180° (for (001)-/(101)-oriented films) and 90° multi-step switching (for (111)-oriented films) and these processes are subsequently observed in stroboscopic piezoresponse force microscopy. These results have implications for our understanding of ferroelectric switching and offer

opportunities to change domain reversal speed. Our work also offers new insights into the microscopic origin of dielectric enhancement and provides a pathway to engineer the dielectric response of these materials.

5.2 Suggestions for Future work

1, Although we have observed large dielectric response from the volume of large density of 90° domain walls in (111)-oriented films, It is noted that the extrinsic motional response in (111)-oriented films has been turned off due to the degeneracy nature of domain variants in such orientation. Thus to ultimately maximize the dielectric response in (111)-oriented films, it is important to turn on the extrinsic motional response. The key to turn on such response is to break the degeneracy of polarization variants. One can introduce anisotropic strain from substrates to break the domain degeneracy thus to turn on the extrinsic response and increase the total dielectric response in (111)-oriented films.

2, So far all the dielectric property characterizations are carried out on macroscopic capacitor structures, which will measure the properties from the materials under the whole capacitor electrode. The minimum probing size depends on the size of electrode, which is usually around μm scale. This adds more challenges to separate out the response from domain and domain wall regions due to the nanoscale size of these structures. To directly probe the property from these nanoscale structures, one can utilize another technique so called band excitation non-linearity PFM and band excitation switching spectroscopy to investigate the local response and switching behavior. All these techniques, originally developed in Oak Ridge National Lab, now have been commercialized as a module in scanning probe software.

3, In the present work, we have specifically investigated the effects of film orientation on the dielectric susceptibilities and developed a more comprehensive GLD model that allow us to consider the effects of film orientation, epitaxial strain, and film composition. One can also further incorporate another important parameter – film thickness into the present model by introducing strain relaxation by the dislocation and domain formation.

REFERENCES

1. Hoffman, J. et al. Ferroelectric Field Effect Transistors for Memory Applications. *Adv. Mater.* **22**, 2957-2961 (2010).
2. Scott, J. F. Applications of Modern Ferroelectrics. *Science* **315**, 954-959 (2012).
3. Chanthbouala, A. et al. Solid-state memories based on ferroelectric tunnel junctions. *Nature Nanotechnol.* **7**, 101-104 (2012).
4. Eom, C.B. & Trolier-McKinstry, S. Thin-film piezoelectric MEMS. *MRS Bull.* **37**, 1007-1021 (2012).
5. Wessels, B.W. Ferroelectric epitaxial thin-films for integrated optics. *Annu. Rev. Mater. Res.* **37**, 659-679 (2007).
6. Lee, D. et al. Multilevel data storage memory using deterministic polarization control. *Adv. Mater.* **24,** 402-406 (2012).
7. Muralt, P. Ferroelectric thin films for micro-sensors and actuators: a review. *J. Micromech. Microeng.* **10,** 136-146 (2000).
8. Saito, Y. et al. Lead-free piezoceramics. *Nature* **432,** 84-87 (2004).
9. Lang, S.B. Pyroelectricity: From ancient curiosity to modern imaging tool. *Phys. Today* **58,** 31-36 (2005).
10. Whatmore, R.W. Pyroelectric devices and materials. *Rep. Prog. Phys.* **49,** 1335-1386 (1986).
11. Whatmore, R.W., Patel, A., Shorrocks, N.M. & Ainger, F.W. Ferroelectric materials for thermal IR sensors state-of-the-art and perspectives. *Ferroelectrics* **104,** 269-283 (1990).
12. Zhang, Q.M., Wang, H., Kim, N. & Cross, L.E. Direct evaluation of domain-wall and intrinsic contributions to the dielectric and piezoelectric response and their temperature dependence on lead zirconate-titanate ceramics. *J. Appl. Phys.* **75,** 454-459 (1994).
13. Taylor, D.V. & Damjanovic, D. Evidence of domain wall contribution to the dielectric permittivity in PZT thin films at sub-switching fields. *J. Appl. Phys.* **82,** 1973-1975 (1997).
14. Randall, C.A., Kim, N., Kucera, J. P., Cao, W. W. & Shrout, T.R. Intrinsic and Extrinsic Size Effects in Fine-Grained Morphotropic-Phase-Boundary Lead Zirconate Titanate Ceramics. *J. Am. Ceram. Soc.* **81,** 677-688 (1998).
15. Hall, D.A. & Stevenson, P.J. High field dielectric behaviour of ferroelectric ceramics. *Ferroelectrics* **228,** 139-158 (1999)
16. Xu, F. et al. Domain wall motion and its contribution to the dielectric and piezoelectric properties of lead zirconate titanate films. *J. Appl. Phys.* **89,** 1336-1348 (2001).
17. Setter, N. et al. Ferroelectric thin films: Review of materials, properties, and applications. *J. Appl. Phys.* **100,** 051606 (2006).
18. Bassiri-Gharb, N. et al. Domain wall contributions to the properties of piezoelectric thin films. *J. Electroceram.* **19,** 47-65 (2007).
19. Karthik, J., Damodaran, A.R. & Martin, L.W. Effect of 90° domain walls on the low-field permittivity of $PbZr_{0.2}Ti_{0.8}O_3$ thin films. *Phys. Rev. Lett.* **108,** 167601 (2012).
20. Karthik, J., Agar, J.C., Damodaran, A.R. & Martin, L.W. Effect of 90° domain walls and thermal expansion mismatch on the pyroelectric properties of epitaxial $PbZr_{0.2}Ti_{0.8}O_3$ thin films. *Phys. Rev. Lett.* **109,** 257602 (2012).
21. Lawless, W.N. & Fousek, J. Small-signal permittivity of the stationary (100)-180^o domain wall in $BaTiO_3$. *J. Phys. Soc. Jpn.* **28,** 419-424 (1970).
22. Rao, W. F. & Wang, Y.U. Domain wall broadening mechanism for domain size effect of enhanced piezoelectricity in crystallographically engineered ferroelectric single crystals. *Appl. Phys. Lett.* **90,** 041915 (2007).
23. Hlinka, J., Ondrejkovic, P. & Marton, P. The piezoelectric response of nanotwinned $BaTiO_3$. *Nanotechnology* **20,** 105709 (2009).

24. Morozovska, A.N., Eliseev, E.A., Varenyk, O.V. & Kalinin, S.V. Effective piezoelectric response of twin walls in ferroelectrics. *J. Appl. Phys.* **113,** 187222 (2013).
25. Fousek, J. The contribution of domain walls to the small-signal complex permittivity of $BaTiO_3$. *Czech J Phys* **15,** 412-417 (1965).
26. Nettleton, R.E. Switching resonance in crystallites of barium titanate. *J. Phys. Soc. Jpn.* **21,** 1633-1639 (1966).
27. Lawless, W.N. 180° Domain-wall energies in $BaTiO_3$. *Phys. Rev.* **175,** 619-624 (1968).
28. Dawber, M., Rabe, K.M. & Scott, J.F. Physics of thin-film ferroelectric oxides. *Rev. Mod. Phys.* **77**, 1083-1130 (2005).
29. Martin, L.W. & Schlom, D.G. Advanced synthesis techniques and routes to new single-phase multiferroics. *Curr. Opin. Solid State Mater. Sci.* **16**, 199-215 (2012).
30. Nagarajan, V. et al. Thickness dependence of structural and electrical properties in epitaxial lead zirconate titanate films. *J. Appl. Phys.* **86**, 595-602 (1999).
31. Li, Y.L., Hu, S.Y., Liu, Z.K. & Chen, L.Q. Effect of electrical boundary conditions on ferroelectric domain structures in thin films. *Appl. Phys. Lett.* **81**, 427-429 (2002).
32. Pertsev, N.A., Arlt, G. & Zembilgotov, A.G. Domain-wall and intrinsic contributions to the dielectric response of epitaxial ferroelectric films. *Microelectron. Eng.* **29**, 135-140 (1995).
33. Kim, D.J., Maria, J.P., Kingon, A.I. & Streiffer, S.K. Evaluation of intrinsic and extrinsic contributions to the piezoelectric properties of $Pb(Zr_{1-x}Ti_x)O_3$ thin films as a function of composition. *J. Appl. Phys.* **93**, 5568-5575 (2003).
34. Bruchhaus, R., Pitzer, D., Schreiter, M. & Wersing, W. Optimized PZT thin films for pyroelectric IR detector arrays. *J. Electroceram.* **3**, 151-162 (1999).
35. Karthik, J. & Martin, L.W. Pyroelectric properties of polydomain epitaxial $Pb(Zr_{1-x}Ti_x)O_3$ thin films. *Phys. Rev. B* **84**, 024102 (2011).
36. Pertsev, N.A., Kukhar, V.G., Kohlstedt, H. & Waser, R. Phase diagrams and physical properties of single-domain epitaxial $Pb(Zr_{1-x}Ti_x)O_3$ thin films. *Phys. Rev. B* **67**, 054107 (2003).
37. Pertsev, N.A. & Zembilgotov, A.G. Domain populations in epitaxial ferroelectric thin films: Theoretical calculations and comparison with experiment. *J. Appl. Phys.* **80**, 6401-6406 (1996).
38. Saito, K., Kurosawa, T., Akai, T., Oikawa, T. & Funakubo, H. Structural characterization and 90 degrees domain contribution to ferroelectricity of epitaxial $Pb(Zr_{0.35},Ti_{0.65})O_3$ thin films. *J. Appl. Phys.* **93**, 545-550 (2003).
39. Oikawa, T., Aratani, M., Funakubo, H., Saito, K. & Mizuhira, M. Composition and orientation dependence of electrical properties of epitaxial $Pb(Zr_xTi_{1-x})O_3$ thin films grown using metalorganic chemical vapor deposition. *J. Appl. Phys.* **95**, 3111-3115 (2004).
40. Bernal, A., Zhang, S.J. & Bassiri-Gharb, N. Effects of orientation and composition on the extrinsic contributions to the dielectric response of relaxor-ferroelectric single crystals. *Appl. Phys. Lett.* **95**, 142911 (2009).
41. Wada, S., Yako, K., Kakemoto, H., Tsurumi, T. & Kiguchi, T. Enhanced piezoelectric properties of barium titanate single crystals with different engineered-domain sizes. *J. Appl. Phys.* **98**, 014109 (2005).
42. Nagarajan, V. et al. Thickness dependence of structural and electrical properties in epitaxial lead zirconate titanate films. *J. Appl. Phys.* **86,** 595-602 (1999).
43. Ouyang, J. et al. Engineering of self-assembled domain architectures with ultra-high piezoelectric response in epitaxial ferroelectric films. *Adv. Funct. Mater.* **17,** 2094-2100 (2007).
44. Romanov, A.E., Vojta, A., Pompe, W., Lefevre, M.J. & Speck, J.S. Domain patterns in (111) oriented tetragonal ferroelectric films. *Phys. Status Solidi A* **172,** 225-253 (1999).
45. Tanaka, M. & Honjo, G. Electron Optical Studies of Barium Titanate Single Crystal Films. *J. Phys. Soc. Jpn.* **19,** 954-970 (1964).
46. Dennis, M.D. & Bradt, R.C. Thickness of 90^o ferroelectric domain walls in $(Ba,Pb)TiO_3$ single crystals. *J. Appl. Phys.* **45,** 1931-1933 (1974).

47. Tsai, F., Khiznichenko, V. & Cowley, J.M. High-resolution electron microscopy of 90° ferroelectric domain boundaries in $BaTiO_3$ and $Pb(Zr_{0.52}Ti_{0.48})O_3$. *Ultramicroscopy* **45,** 55-63 (1992).
48. Floquet, N. & Valot, C. Ferroelectric domain walls in $BaTiO_3$: Structural wall model interpreting fingerprints in XRPD diagrams. *Ferroelectrics* **234,** 107-122 (1999).
49. Venkatesan, S., Kooi, B. J., De Hosson, J. T., Vlooswijk, A. H. G. & Noheda, B. Substrate influence on the shape of domains in epitaxial $PbTiO_3$ thin films. *J. Appl. Phys.* **102,** 104105 (2007).
50. Schlom, D.G. et al. Strain tuning of ferroelectric thin films. *Annu. Rev. Mater. Res.* **37,** 589-626 (2007).
51. Cross, E. Materials science: Lead-free at last. *Nature* **432,** 24-25 (2004).
52. Koukhar, V.G., Pertsev, N.A. & Waser, R. Thermodynamic theory of epitaxial ferroelectric thin films with dense domain structures. *Phys. Rev. B* **64,** 214103 (2001).
53. Kukhar, V.G., Pertsev, N.A., Kohlstedt, H. & Waser, R. Polarization states of polydomain epitaxial $Pb(Zr_{1-x}Ti_x)O_3$ thin films and their dielectric properties. *Phys. Rev. B* **73,** 214103 (2006).
54. Tagantsev, A.K., Pertsev, N.A., Muralt, P. & Setter, N. Strain-induced diffuse dielectric anomaly and critical point in perovskite ferroelectric thin films. *Phys. Rev. B* **65,** 012104 (2001).
55. Pertsev, N.A. & Koukhar, V.G. Polarization instability in polydomain ferroelectric epitaxial thin films and the formation of heterophase structures. *Phys. Rev. Lett.* **84,** 3722-3725 (2000).
56. Du, X. H., Zheng, J., Belegundu, U. & Uchino, K. Crystal orientation dependence of piezoelectric properties of lead zirconate titanate near the morphotropic phase boundary. *Appl. Phys. Lett.* **72,** 2421-2423 (1998).
57. Du, X. H., Belegundu, U. & Uchino, K. Crystal orientation dependence of piezoelectric properties in lead zirconate titanate: theoretical expectation for thin films. *Jpn. J. Appl. Phys.* **36,** 5580-5587 (1997).
58. Wada, S. et al. Domain wall engineering in lead-free piezoelectric crystals. *Ferroelectrics* **355,** 37-49 (2007).
59. Wada, S., Yako, K., Yokoo, K., Kakemoto, H. & Tsurumi, T. Domain wall engineering in barium titanate single crystals for enhanced piezoelectric properties. *Ferroelectrics* **334,** 17-27 (2006).
60. Saito, K., Kurosawa, T., Oikawa, T., & Funakubo, H. Structural characterization and 90° domain contribution to ferroelectricity of epitaxial $Pb(Zr_{0.35},Ti_{0.65})O_3$ thin films, *J. Appl. Phys.* **93,** 545-550 (2003).
61. Hlinka, J. & Márton, P. Phenomenological model of a 90° domain wall in $BaTiO_3$-type ferroelectrics. *Phys. Rev. B* **74,** 104104 (2006).
62. Scrymgeour, D.A. & Gopalan, V. Nanoscale piezoelectric response across a single antiparallel ferroelectric domain wall. *Phys. Rev. B* **72,** 024103 (2005).
63. Morozovska, A.N., Eliseev, E.A., Bravina, S.L. & Kalinin, S.V. Resolution-function theory in piezoresponse force microscopy: Wall imaging, spectroscopy, and lateral resolution. *Phys. Rev. B* **75,** 174109 (2007).
64. Karthik, J., Damodaran, A.R. & Martin, L.W. Epitaxial ferroelectric heterostructures fabricated by selective area epitaxy of $SrRuO_3$ using an MgO mask. *Adv. Mater.* **24**, 1610-1615 (2012).
65. Kamel, T. M., de With, G. Double peak switching current in soft ferroelectric lead zirconate titanate. *J. Appl. Phys.* **102**, 044118 (2007).
66. Yin, J., Cao, W. Polarization reversal study using ultrasound. *Appl. Phys. Lett.* **79**, 4556-4558 (2001).
67. Daniels, J. E., Finlayson, T. R., Davis, M., Damjanovic, D., Studer, A. J., Hoffman, M. & Jones, J. L. Neutron diffraction study of the polarization reversal mechanism in $[111]_C$-oriented $Pb(Zn_{1/3}Nb_{2/3})O_3$-x$PbTiO_3$. *J. Appl. Phys.* **101**, 104108 (2007).
68. Pramanick, A., Prewitt, A. D., Forrester, J. S. & Jones, J. L. Domains, domain walls and defects in perovskite ferroelectric oxides: A review of present understanding and recent contributions. *Crit. Rev. Solid State Mater. Sci.* **37**, 243-275 (2012).

69. Nagarajan, V., Roytburd, A., Stanishevsky, A., Prasertchoung, S., Zhao, T., Chen, L. Q., Meingailis, J., Auciello, O. & Ramesh, R. Dynamics of ferroelastic domains in ferroelectric thin films. *Nature Mater*. **2**, 43-47 (2003).
70. Anbusathaiah, V., Kan, D., Kartawidjaja, F. C., Mahjoub, R., Arredondo, M. A., Wicks, S., Takeuchi, I., Wang, J. & Nagarajan, V. Labile ferroelastic nanodomains in bilayered ferroelectric thin films. *Adv. Mater.* **21**, 3497-3502 (2009).
71. Meyer, B. & Vanderbilt, D. *Ab initio* study of ferroelectric domain walls in $PbTiO_3$. *Phys. Rev. B* **65**, 104111 (2002).
72. Gao, P., Britson, J., Jokisaari, J. R., Nelson, C. T., Baek, S.-H., Wang, Y., Eom, C.-B., Chen, L.-Q. & Pan, X. Atomic-scale mechanisms of ferroelastic domain-wall-mediate ferroelectric switching. *Nature Commun.* **4**, 2791 (2013).